

# Structure learning for zero-inflated counts, with an application to single-cell RNA sequencing data

NGUYEN THI KIM HUE

*Department of Statistical Sciences, University of Padova, Padova, Italy.*

KOEN VAN DEN BERGE

*Department of Statistics, University of California, Berkeley, Berkeley, CA, USA.  
Department of Applied Mathematics, Computer Science and Statistics, Ghent University,  
Ghent, Belgium.*

MONICA CHIOGNA

*Department of Statistical Sciences, University of Bologna, Italy.*

DAVIDE RISSO\*

*Department of Statistical Sciences, University of Padova, Padova, Italy.  
davide.risso@unipd.it*

## SUMMARY

The problem of estimating the structure of a graph from observed data is of growing interest in the context of high-throughput genomic data, and single-cell RNA sequencing in particular. These, however, are challenging applications, since the data consist of high-dimensional counts with high variance and over-abundance of zeros. Here, we present a general framework for learning the structure of a graph from single-cell RNA-seq data, based on the zero-inflated negative binomial distribution. We demonstrate with simulations that our approach is able to retrieve the structure of a graph in a variety of settings and we show the utility of the approach on real data.

*Key words:* graphical models, structure learning, single cell, RNA sequencing, zero inflation, count data

## 1. STRUCTURE LEARNING AND OMICS TECHNOLOGIES: THE INTERPLAY

In recent years, a growing interest has developed around the problem of retrieving, starting from observed data, the structure of graphs representing relationships among variables of interest. In fact, reconstruction of a graphical model, known as structure learning, traces back to the beginning of the nineties, and a vast literature exists that considers the problem from various perspectives, within both frequentist and Bayesian approaches (see Drton and Maathuis (2017) for an extensive review). But a central role in the renewal of interest on structure learning

\*To whom correspondence should be addressed.

has been played by molecular biology applications. In this field, the abundance of data with increasingly large sample sizes, driven by novel high-throughput technologies, has opened the door for the development and application of structure learning methods, in particular applied to the estimation of gene regulatory or gene association networks.

At the inception of transcriptomics, the technology of choice for measuring gene expression was the microarray assay, that, by optically scanning fluorophore intensities, provided data on a continuous scale (Irizarry *and others*, 2003). When it came to (sparse) structure learning from these data, the first proposals assumed that data arose from a multivariate Gaussian distribution, and took advantage of the many results and tools available for such family of distributions (see Schäfer and Strimmer (2005); Junbai *and others* (2005); Peña (2008); Yin and Li (2011), among others).

Later, a new technology allowed for the high-throughput sequencing of RNA molecules (i.e., RNA-seq), and quickly established itself as the reference technology for the study of genome-wide transcription levels (Wang *and others*, 2009). One of the main advantages of RNA-seq over microarrays is that it allows to analyze small amounts of RNA, making it feasible to study gene expression even at single-cell resolution (Kolodziejczyk *and others*, 2015). This new technology provided statisticians with a wealth of novel problems. Indeed, RNA-seq yields counts, rather than intensities on a continuous scale, as measures of gene expression. Data are usually high dimensional and, typically, come from skewed distributions with high variance. Moreover, they very often show a large number of zeros, typically larger than expected under a Poisson model (Van De Wiel *and others*, 2013).

Structure learning of graphs with such data was initially performed by exploiting data transformations, such as log, Box-Cox, copulas, etc (Abegaz and Wit, 2015). Although data transformation can work well in some circumstances, it can be also ill-suited, possibly leading to wrong inferences in some circumstances (Gallopín *and others*, 2013). Awareness of these problems fueled the development of methods for learning (sparse) graphical models tailored to count data. Allen and Liu (2013), Yang *and others* (2013) and, more recently, Nguyen and Chiogna (2018) considered structure learning for Poisson and truncated Poisson counts. A general class of models was studied in Yang *and others* (2015), which considered graphical models for the class of exponential distributions.

The challenges posed by RNA-seq technology are exacerbated in single-cell RNA sequencing (scRNA-seq). scRNA-seq allows the measurement of RNA from individual cells, promising to permit the study of gene interactions at an unprecedented resolution (McDavid *and others*, 2019). Two platforms are emerging as state-of-the-art scRNA-seq technologies: (i) plate-based *full-length* protocols (e.g., Picelli *and others*, 2014), and (ii) *droplet*-based protocols (e.g., Macosko *and others*, 2015; Zheng *and others*, 2017). Droplet methods allow to process thousands of cells at a time, while full-length studies are typically limited to hundreds of cells. Furthermore, droplet methods employ *unique molecular identifiers*, which help reduce amplification biases (Islam *and others*, 2014), while full-length protocols typically do not. These features make the distribution of the resulting data substantially different: full-length data typically show larger counts than droplet methods and a more pronounced bi-modality (Svensson, 2020). Moreover, the small amount of RNA present in the cell and the technical limitations of the sequencing platforms (e.g., a limited number of sequenced *reads* per cell) lead to higher variance and larger fraction of zero counts compared to “bulk” RNA-seq (Risso *and others*, 2018; McDavid *and others*, 2019). As a result, single-cell RNA-seq gene-wise data distributions are highly skewed and show an abundance of zero counts. Inference using Gaussian models is definitely infeasible even after variance stabilizing transformations and even models for count data may suffer from high false discovery rates (see Section 6). To account for zero-inflation, McDavid *and others* (2019) proposed a Hurdle model,

equivalent to a finite mixture of singular Gaussian distributions. The authors’ model, however, does not account for the count nature of the data.

From this quick tour on problems and methods, it appears evident that principled solutions to structure learning that account for the possibility of over-dispersion and/or zero-inflation are still lacking. In this paper, we try to fill this gap. We present a general framework, based on the zero-inflated negative binomial distribution, for learning the structure of a graph from single-cell RNA-seq data. We focus in particular on droplet data, for two reasons: (i) its growing popularity suggests that the majority of future studies will employ this protocol; (ii) given the high dimensionality of the problem, it is desirable to have a large sample size and droplet protocols allow the sequencing of more cells.

The remainder of this article is organized as follows. In Section 2 we introduce a motivating dataset; we describe our proposed model in Section 3 and our structure learning procedure in Section 4. One key question in the literature is whether zero inflation needs to be accounted for in the data, we offer our perspective in Section 5. After exploring the behavior of our method in simulated data in Section 6, we apply our proposal to real single-cell RNA-seq data in Section 7. Section 8 concludes the article with a discussion.

## 2. A MOTIVATING EXAMPLE: SINGLE-CELL GENE EXPRESSION IN THE OLFACTORY EPITHELIUM

Despite the distributional challenges described in the previous section, single-cell data offer an unprecedented opportunity to discover cellular dynamics, especially in developing cell populations. Here, we study gene expression from the mouse olfactory epithelium (OE). This tissue is made of two major mature cell types, olfactory neurons and sustentacular support cells. Furthermore, a stem cell niche provides a mechanism through which the tissue is regenerated (Fletcher *and others*, 2017; Gadye *and others*, 2017). As the aim of the study is to understand how stem cells mature into neurons following tissue damage, we focused only on the cells in the neuronal lineage. Briefly, the olfactory reserve stem cells, called Horizontal Basal Cells (HBC), become activated and subsequently develop into Globose Basal Cells (GBC) and then into immature (iOSN) and finally mature olfactory neurons (mOSN). By reconstructing the structure of the graph for each of these cell types separately, we hope to get a glimpse of the dynamic relationships between genes in neuronal development.

To this aim, we analyzed a set of 17,743 cells, assayed with 10X Genomics (v2 chemistry) after injury of the OE, to characterize HBCs and their descendants during regeneration (Brann *and others*, 2020). Starting from an initial set of 25,469 cells, low-quality samples as well as potential doublets were removed as described in Brann *and others* (2020). After clustering with the Leiden algorithm (Traag *and others*, 2019), known marker genes were used to identify cell types. We discarded the cell types outside of the neuronal lineage (macrophages, sustentacular cells, and microvillar cells), obtaining our final dataset consisting of 7782 HBCs, 5418 activated HBCs (HBC\*), 755 GBCs, 2859 iOSN, and 929 mOSN. For more details on the data preprocessing, see Brann *and others* (2020).

## 3. MODEL SPECIFICATION

### 3.1 Preliminaries

A probabilistic graphical model requires the definition of a pair,  $(G, \mathcal{F})$  say. Here,  $G = (V, E)$  represents an undirected graph, where  $V$  is the set of nodes, and  $E = \{(s, t) : s, t \in V, s \neq t\}$  represents the set of undirected edges. Each node in the graph corresponds to a random variable

$X_s, s \in V$ ; the existence of an edge  $(s, t) \in E$  indicates the dependency of the random variables  $X_s$  and  $X_t$ . Moreover,  $\mathcal{F}$  represents a family of probability measures for the random vector  $\mathbf{X}_V$ , indexed by  $V$  and with support  $\mathcal{X}_V$ .

Thanks to the well known Markov properties (global, local, pairwise, see Lauritzen (1996)), the pattern of edges in the graph translates into conditional independence properties for variables in  $\mathbf{X}_V$ , which, in turn, allow possible factorizations of  $\mathcal{F}$  into smaller, more tractable entities. In undirected graphical models, each absent edge  $(s, t)$  in  $E$  has the role of portraying the conditional independence,

$$X_s \perp\!\!\!\perp X_t | \mathbf{X}_{V \setminus \{s, t\}},$$

and the family  $\mathcal{F}$  is said to satisfy the pairwise Markov property with respect to  $G$ . The smallest undirected graph  $G$  with respect to which  $\mathcal{F}$  is pairwise Markov is given the name conditional independence graph.

When all variables in  $\mathbf{X}_V$  are discrete with positive joint probabilities, as is the case of this paper, the three kinds of Markov properties are equivalent, so that a factorization of the joint probability distribution with respect to the cliques (fully connected subsets of vertices) of the graph  $G$  is also guaranteed (Lauritzen, 1996, Chap. 3).

### 3.2 The model specification

Here, we assume that the distribution of each variable  $X_s$ , conditional to all possible subsets of variables  $\mathbf{X}_K, K \subseteq V$  is a zero-inflated negative binomial (zinb) distribution:  $X_s | \mathbf{X}_{K \setminus \{s\}} \sim \text{zinb}(x_s; \mu_{s|K}, \theta_s, \pi_{s|K} | \mathbf{X}_{K \setminus \{s\}})$ , i.e.,

$$f_{\text{zinb}}(x_s; \mu_{s|K}, \theta_s, \pi_{s|K} | \mathbf{X}_{K \setminus \{s\}}) = \pi_{s|K} \delta_0(x_s) + (1 - \pi_{s|K}) f_{\text{nb}}(x_s, \mu_{s|K}, \theta_s | \mathbf{X}_{K \setminus \{s\}}), \quad (3.1)$$

where  $\delta_0(\cdot)$  is the Dirac function,  $\pi_{s|K} \in [0, 1]$  is the probability that a 0 is sampled from a distribution degenerate at zero and  $f_{\text{nb}}(\cdot, \mu, \theta)$  denotes the probability mass function of the negative binomial (NB) distribution with mean  $\mu$  and inverse dispersion parameter  $\theta$ . We assume that

$$\ln(\mu_{s|K}) = \nu_{s|K}^\mu + \sum_{t \in K \setminus \{s\}} \beta_{st|K}^\mu x_t, \quad (3.2)$$

$$\text{logit}(1 - \pi_{s|K}) = \nu_{s|K}^\pi + \sum_{t \in K \setminus \{s\}} \beta_{st|K}^\pi x_t. \quad (3.3)$$

When both  $\mu_{s|K}$  and  $\pi_{s|K}$ , are not constant, a missing edge between node  $s$  and node  $t$  corresponds to the condition  $\beta_{st|K}^\mu = \beta_{ts|K}^\mu = \beta_{st|K}^\pi = \beta_{ts|K}^\pi = 0, \forall K \subseteq V \setminus \{s\}$ . On the other hand, one edge between node  $s$  and node  $t$  implies that at least one of four parameters  $\beta_{st|K}^\mu, \beta_{ts|K}^\mu, \beta_{st|K}^\pi, \beta_{ts|K}^\pi$  is different from 0.

This specification defines a family of models that includes the most common models employed with count data and embraces a variety of situations. A priori, the zinb model holds no particular rank in this family, but it is a convenient starting point from which the family of models can be established. It is quite evident that, when  $\pi_{s|K} = 0, \forall K \subseteq V \setminus \{s\}$ , the model reduces to a negative binomial distribution, which, in turn reduces to a Poisson distribution when the inverse dispersion parameter  $\theta_s$  tends to infinity. When  $\pi_{s|K} > 0$ , zero-inflation comes into play and zero-inflated Poisson and negative binomial models can be considered. In this case, when  $\beta_{st|K}^\pi = 0, \forall t \in K \setminus \{s\}$ , the neighborhood of a node  $s$  is defined to be the set of effective predictors of  $\mu_{s|K}$

and consists of all nodes  $t$  for which  $\beta_{st|K}^\mu \neq 0$ . On the other side, when  $\beta_{st|K}^\mu = 0, \forall t \in K \setminus \{s\}$ , the neighborhood of a node  $s$  is defined to be the set of effective predictors of  $\pi_{s|K}$  and consists of all nodes  $t$  for which  $\beta_{st|K}^\pi \neq 0$ . In other words, the family includes models in which the structure of the graph is attributable only to one of the two parameter components,  $\pi_{s|K}$  or  $\mu_{s|K}$ .

The difficulty with our model specification is that the definition of a set of conditional distributions does not guarantee the existence of a valid joint distribution, i.e., a joint distribution that possesses the specified conditionals. This might create difficulties in interpreting the resulting graph in probabilistic terms: if the joint distribution does not exist, graphical separations stored in  $G$  as a result of our model specification might not correspond to conditional independence properties on  $\mathcal{F}$ . However, our formulation guarantees existence of the joint distribution in a number of relevant subcases. In the following theorem, we clarify conditions for existence of a joint distribution coherent with the conditional specification (see Section 1.1, Supplementary Material, for a proof).

**THEOREM 3.1** Let  $\mathbf{X}_V = (X_1, X_2, \dots, X_p)$  be a  $p$ -random vector with support  $\mathcal{X}_V$ . Assume that a set of univariate conditional probability mass functions of kind (3.1) are given for variables in  $\mathbf{X}_V$ . Then, a joint distribution having those conditionals exists if and only if  $\theta_s$  is constant for all  $s \in V$ , and all regression coefficients  $\beta_{st|K}^\mu$  are negative,  $\forall K \subseteq V$ .

The condition on negativity of local regression coefficients in (3.2) resembles a condition known in the literature of Markov random fields known as “competitive relationship” (Besag, 1974). Generally speaking, the presence of only negative relations among entities is quite a rare event and incapability of capturing positive dependencies might be a severe drawback in various applications. Nevertheless, the existence of a joint distribution in these specific cases assures that statistical guarantees hold for conditional approaches to structure learning such as the one used in this paper and somehow softens the hazard of the use of such algorithms outside the conditions of existence of a joint distribution.

#### 4. STRUCTURE LEARNING

A conditional independence graph  $G = (V, E)$  on  $\mathbf{X}_V$  can be estimated by estimating, for each node  $s \in V$ , its neighborhood. Hence, one can proceed by estimating the conditional distribution of  $X_s | \mathbf{X}_{V \setminus s}$  and fixing the neighborhood of  $s$  to be the index set of variables  $\mathbf{X}_{N(s)}$  on which the conditional distribution depends.

To estimate the neighborhood of each node, we employ the PC-stable algorithm, a variant of the PC algorithm first proposed by Spirtes *and others* (2000). The PC algorithm starts with a complete graph on  $V$ . Marginal independencies for all pairs of nodes are tested, and edges removed when marginal independencies are found. Then, for every pair of linked nodes, independence is tested conditional to all subsets of cardinality one of the adjacency sets of the two nodes. This testing procedure is iterated, increasing in turn the size of the conditioning sets, until this reaches its maximum limit, or a limit imposed by the user. Reasons for choosing the PC algorithm are many, spanning from its consistency (assuming no latent confounders) under i.i.d. sampling (Spirtes *and others*, 2000), to its ability to deal with a large number of variables and only moderately large sample sizes. The variant that we employ, PC-stable (Colombo and Maathuis, 2014), allows to control instabilities due to the order in which the conditional independence tests are performed. To perform the tests, deviance test statistics are employed, for which a chi-squared asymptotic distribution can be obtained by standard asymptotic theory.

In what follows, let  $\mathbb{X} = \{\mathbf{x}^{(1)}, \dots, \mathbf{x}^{(n)}\}$  be the collection of  $n$  samples drawn from the random vectors  $\mathbf{X}_V$ , with  $\mathbf{x}^{(i)} = (x_{i1}, \dots, x_{ip})$ ,  $i = 1, \dots, n$ . For each  $K \subseteq V$ , let  $\mathbb{X}_K$  be the set of  $n$  samples of the  $|K|$ -random vector  $\mathbf{X}_K = (X_t : t \in K)$ , with  $\mathbf{x}_K^{(i)} = (x_{it})_{t \in K}$ ,  $i = 1, \dots, n$ . Starting from the complete graph, for each  $s$  and  $t \in V \setminus \{s\}$  and for any set of variables  $\mathbf{S} \subseteq \{1, \dots, p\} \setminus \{s, t\}$ , we test, at some pre-specified significance level, the null hypothesis  $H_0 : \beta_{st|K}^\mu = \beta_{ts|K}^\mu = \beta_{st|K}^\pi = \beta_{ts|K}^\pi = 0$ , with  $K = \mathbf{S} \cup \{s, t\}$ . In other words, we test if the data support the existence of the conditional independence relation  $X_s \perp\!\!\!\perp X_t | \mathbf{X}_\mathbf{S}$ . If the null hypothesis is not rejected, the edge  $(s, t)$  is considered to be absent from the graph. A control is operated on the cardinality of the set  $\mathbf{S}$  of conditioning variables, which is progressively increased from 0 to  $p - 2$  or to  $m$ ,  $m < (p - 2)$ .

Assume  $X_s | \mathbf{x}_{K \setminus \{s\}} \sim \text{zinh}(X_s; \mu_{s|K}, \theta_s, \pi_{s|K} | \mathbf{x}_{K \setminus \{s\}})$ , as in Equation (3.1). The conditional log-likelihood for variable  $X_s$  given  $\mathbf{x}_{K \setminus \{s\}}$  is obtained by

$$\ell_s(\boldsymbol{\nu}_{s|K}, \boldsymbol{\beta}_{s|K}, \theta_s) = \sum_{i=1}^n \ln f_{\text{zinh}}(x_{is}; \mu_{s|K}, \theta_s, \pi_{s|K} | \mathbf{x}_{K \setminus \{s\}}^{(i)}), \quad (4.4)$$

where  $\boldsymbol{\nu}_{s|K}, \boldsymbol{\beta}_{s|K}$  are linked to  $\boldsymbol{\pi}_{s|K}, \boldsymbol{\mu}_{s|K}$  through Equations (3.2) – (3.3). The estimates  $\hat{\boldsymbol{\nu}}_{s|K}, \hat{\boldsymbol{\beta}}_{s|K}, \hat{\theta}_s$  of the parameters  $\boldsymbol{\nu}_{s|K}, \boldsymbol{\beta}_{s|K}, \theta_s$  are obtained by maximizing the conditional log-likelihood given in Equation (4.4), i.e.,

$$(\hat{\boldsymbol{\nu}}_{s|K}, \hat{\boldsymbol{\beta}}_{s|K}, \hat{\theta}_s) = \operatorname{argmax}_{(\boldsymbol{\nu}_{s|K}, \boldsymbol{\beta}_{s|K}, \theta_s) \in \mathbb{R}^{2|K|+1}} \ell_s(\boldsymbol{\nu}_{s|K}, \boldsymbol{\beta}_{s|K}, \theta_s).$$

See Section 1.2, Supplementary Material, for details on the estimation procedure. A deviance test statistic for the hypothesis  $H_0 : \beta_{st|K}^\mu = \beta_{st|K}^\pi = 0$  can be obtained as

$$D_{s|K} = 2(\ell_s(\hat{\boldsymbol{\nu}}_{s|K}, \hat{\boldsymbol{\beta}}_{s|K}, \hat{\theta}_s) - \ell_s(\hat{\boldsymbol{\nu}}_{s|K}^0, \hat{\boldsymbol{\beta}}_{s|K}^0, \hat{\theta}_s^0)),$$

where  $\hat{\boldsymbol{\nu}}_{s|K}^0, \hat{\boldsymbol{\beta}}_{s|K}^0, \hat{\theta}_s^0$  are the maximum likelihood estimates of the parameters under  $H_0$ . It is readily available that  $D_{s|K}$  is asymptotically chi-squared distributed with 2-degrees of freedom under the null hypothesis, provided that some general regularity conditions hold.

**Remark 1.** On assuming faithfulness of the node conditional distributions to the graph  $G$ , consistency of the algorithm can be proved in the case of competitive relationships in  $\mu_s | K$  by suitably modifying results in Nguyen and Chiogna (2018). We recall that a distribution  $P_\mathbf{X}$  is said to be faithful to the graph  $G$  if for all disjoint vertex sets  $A, B, C \subset V$  it holds

$$\mathbf{X}_A \perp\!\!\!\perp \mathbf{X}_B | \mathbf{X}_C \Rightarrow A \perp\!\!\!\perp_G B | C,$$

where  $A \perp\!\!\!\perp_G B | C$  means that  $A$  and  $B$  are separated in  $G$  by  $C$ . Thanks to the equivalence between local and global Markov properties, faithfulness of the local distributions guarantees faithfulness of the joint distribution.

**Remark 2.** A large sample size, as typical in the applications at hand, impacts on the actual significance level of individual tests. Moreover, a multiplicity of tests are performed by the algorithm. For this reason, we advice to set the nominal level of the test  $\alpha$  to  $\alpha_n = 2(1 - \Phi(n^b))$ , where  $0 < b < 1/2$  is related to the average neighborhood size. This choice is based on results in Nguyen and Chiogna (2018) and guarantees that the probability that a type I or II error occurs in the whole testing procedure goes to zero as  $n \rightarrow \infty$ , i.e., it asymptotically controls the family-wise error rate of all potential tests that could be done.

**Remark 3.** The chosen learning strategy has some advantages over alternative approaches based on sparse regressions (see also Nguyen and Chiogna (2018) for an extended discussion in the Poisson case). Sparsity can be easily implemented by a control on the conditional set size, instead of a control on parameter magnitudes, which can lead to over-shrinkage. Moreover, it offers computational advantages, especially when sparse networks are the target of inference. Finally, hypothesis testing is scale-invariant, i.e., is not affected by scale transformations of regressors.

### 5. ZERO INFLATION: A REAL ISSUE?

The need for modeling zero-inflation in single cell data is a question at the core of an ongoing debate, with several authors arguing that the negative binomial distribution is sufficient to fit single-cell RNA-seq data when unique molecular identifiers are used (Vieth *and others*, 2017; Townes *and others*, 2019; Svensson, 2020). Indeed, the ability to distinguish between a non zero-inflated distribution and zero-inflated alternatives highly depends on the relative size of the parameters of the distributions.

To gain a better understanding of this problem, we have tried to assess the misspecification cost due to assuming a non zero-inflated distribution when zero inflation is in action. To this aim, we confined ourselves to a univariate case with no covariates, fixed a non zero-inflated model and measured the model misspecification cost occurring when using its zero-inflated counterpart by using the squared Hellinger distance as loss function. Such a loss function should, in principle, indicate, in an inferential sense, how far apart the two distributions are.

To this aim, let  $\mathcal{Y} = \{0, 1, 2, \dots, +\infty\}$  be the support of a discrete variable  $Y$ . We consider for  $Y$  a true probability distribution  $P(y; \phi_0)$ ,  $\phi_0 \in \Phi$ , as well as a family  $\mathcal{F} = \{Q(y; \psi), \psi \in \Psi\}$ ,  $\Phi \subseteq \Psi$ , of zero-inflated versions of the true probability distribution  $P(y; \phi_0)$ . The squared Hellinger distance between two probability distributions  $P$  and  $Q$  is defined as

$$\begin{aligned} d_h^2(P, Q) &= \frac{1}{2} \sum_{y \in \mathcal{Y}} (\sqrt{p_y} - \sqrt{q_y})^2 \\ &= 1 - \sum_{y \in \mathcal{Y}} \sqrt{p_y q_y}, \end{aligned}$$

where  $p_y = P(y; \phi_0)$  and  $q_y = Q(y; \psi)$ .

In particular, assume that  $P$  is a NB distribution with  $\phi_0 = (\mu_0, \theta_0)$  and  $Q$  is a zinb distribution, defined as

$$Q(y; \psi) = \pi \delta_0(0) + (1 - \pi) P(y; \phi_0),$$

with  $\psi = (\phi_0, \pi)$ . Hence, the squared Hellinger distance of  $P$  and  $Q$  can be written as

$$d_h^2(P, Q) = 1 - \sqrt{1 - \pi}(1 - P(0; \phi_0)) - \sqrt{P(0; \phi_0)} \sqrt{\pi + (1 - \pi)P(0; \phi_0)}.$$

Table 1 shows the value of the Hellinger distance in a number of cases. As expected, the distance increases with the probability of zero inflation  $\pi$ . However, when the inverse dispersion parameter  $\theta_0$  and/or the mean  $\mu_0$  are small, the distance between the distributions is small even in the case of moderate to large  $\pi$ . In fact, when  $\mu_0$  and  $\theta_0$  are both small (low mean and high variance) the two distributions are close even when  $\pi = 0.9$ .

As, broadly speaking, maximum likelihood estimators and minimum Hellinger distance estimators are asymptotically equivalent, it emerges that, in inferential terms, the degree of zero inflation of a true model could be difficult to ascertain, as suitable choices of the parameters

of the non contaminated component may possibly absorb the excess of zeros generated by the contamination. This is despite identifiability of the zinb model (see Section 1.3, Supplementary Material, for a proof). These remarks might contribute to the ongoing debate about existence of zero-inflation from a novel perspective.

## 6. SIMULATIONS

We devote this section to the empirical study of consistency of the proposed algorithms. In particular, we concentrate on the ability of proposed methods to recover the true structure of the graphs. We also list the running time of each algorithm. As measures of the test’s accuracy, we adopt three criteria including Precision  $P$ ; Recall  $R$ ; and their harmonic mean, known as  $F_1$ -score, respectively defined as

$$P = \frac{TP}{TP + FP}, R = \frac{TP}{TP + FN}, F_1 = 2 \frac{P \cdot R}{P + R},$$

where TP (true positive), FP (false positive), and FN (false negative) refer to the number of inferred edges (Liu *and others*, 2010).

The considered algorithms are listed below, along with specifications, if needed, of tuning parameters. For all PC-like algorithms, we let the maximum cardinality of conditional independence set be  $m = 8$  for  $p = 10$  and  $m = 3$  for  $p = 100$ .

- **PC-zinb1**: zinb models in which the structure of the graph is attributable to both of the two parameter components  $\mu_{s|K}$  and  $\pi_{s|K}$ ;
- **PC-zinb0**: zinb models in which the structure of the graph is attributable to only the parameter component  $\mu_{s|K}$  and consider  $\pi_{s|K}$  as a constant (i.e.,  $\beta_{st|K}^\pi = 0, \forall t \in K \setminus \{s\}, \forall s \in V$ );
- **PC-nb**: Negative binomial model, i.e., the special case of zinb models where  $\pi_{s|K} = 0$ ;
- **PC-pois**: Poisson model (Nguyen and Chiogna, 2018).

### 6.1 Data generation

For two different cardinalities ( $p = 10$  and  $p = 100$ ), we consider three graphs of different structure: (i) a scale-free graph, in which the node degree distribution follows a power law; (ii) a hub graph, where each node is connected to one of the hub nodes; (iii) a random graph, where the presence of the edges is drawn from independent and identically distributed Bernoulli random variables.

To construct the scale-free and random networks, we employed the R package *igraph* (Csardi *and others*, 2006). For the scale-free networks, we followed the Barabasi-Albert model with constant out-degree of the vertices  $\nu = 2$  for  $p = 10$  and  $\nu = 0.2$  for  $p = 100$ . For the random networks, we followed the Erdos-Renyi model with probability to draw one edge between two vertices  $\gamma = 0.3$  for  $p = 10$  and  $\gamma = 0.03$  for  $p = 100$ . To construct the hub networks, we assumed 2 hub nodes for  $p = 10$ , and 5 hub nodes for  $p = 100$ . See Supplementary Figure S1 and Supplementary Figure S2 for representative plots of the three chosen graphs for  $p = 10$  and  $p = 100$ , respectively.

For the given graphs, 50 datasets were sampled with four different sample sizes,  $n = \{100, 200, 500, 1000\}$  for  $p = 10$ , and three different sample sizes,  $n = \{200, 500, 1000\}$  for  $p = 100$ . To



generate the data, we followed the approach of the Poisson models in Allen and Liu (2013). Let  $\mathbb{X} \in \mathbb{R}^{n \times p}$  be the set of  $n$  independent observations of random vector  $\mathbf{X}$ . Then,  $\mathbb{X}$  is obtained from the following model  $\mathbb{X} = \mathbb{Y}A + \epsilon$ , where  $\mathbb{Y} = (y_{st})$  is an  $n \times (p + p(p-1)/2)$  matrix whose entries  $y_{st}$  are realizations of independent random variables  $Y_{st} \sim \text{zinb}(\mu, \theta, \pi)$  (or  $\text{nbinom}(\mu, \theta)$ ; or  $\text{Pois}(\mu)$ ) and  $\epsilon = (e_{st})$  is an  $n \times p$  matrix with entries  $e_{st}$  which are realizations of random variables  $E_{st} \sim \text{zinb}(\mu_{nois}, \theta, \pi)$  (or  $\text{nbinom}(\mu_{nois}, \theta)$ ; or  $\text{Pois}(\mu_{nois})$ ). This approach leverages the additive property of these distributions and allows us to generate the required dependencies. In particular, let  $B$  be the adjacency matrix of a given true graph, then  $A$  takes the following form  $A = [I_p; P \odot (1_p \text{tri}(B)^T)]^T$ . Here,  $P$  is a  $p \times (p(p-1)/2)$  pairwise permutation matrix,  $\odot$  denotes the elementwise product, and  $\text{tri}(B)$  is the  $(p(p-1)/2) \times 1$  vectorized upper triangular part of  $B$  (Allen and Liu, 2013).

## 6.2 Results

Figures 1 and 2 show the Monte Carlo means of the  $F_1$ -scores for each of the considered methods with  $p = 100$  and low signal-to-noise ratio ( $\mu_{nois} = 0.5$ ), at high ( $\mu = 5$ ) and low ( $\mu = 0.5$ ) mean levels, respectively. Each value is computed as the average of the 50 values obtained by simulating 50 samples for the model corresponding to each network. Monte Carlo means of Precision  $P$ , Recall  $R$ , and  $F_1$ -score are given in Tables S1–S3.

The two values of  $\mu = \{5, 0.5\}$  were chosen to mimic typical values observed in real full-length and droplet-based datasets, respectively. In fact, the mean expression level of transcription factors in the dataset presented in Section 2 is 0.67 (median 0.14), while the mean expression level of transcription factors in a similar experiment performed with a full-length protocol (Fletcher *and others*, 2017) is 32.03 (median 7.89).

These results indicate that the PC-zinb1 algorithm and its variants (PC-zinb0, PC-nb, PC-pois) are consistent in terms of reconstructing the structure from given data. In fact, when the model is correctly specified, the  $F_1$ -scores of the algorithms are close to 1 when  $n \geq 1000$  in all scenarios. This means that the proposed algorithm is able to recover the underlying graph from the given data for both low (Fig. 2) and high (Fig. 1) mean levels.

When the data are generated with a high mean level ( $\mu = 5$ ), the PC-pois algorithm performs well only when it is the true model, i.e., for data generated from Poisson random variables (Fig. 1; Supplementary Table S3). In the other scenarios, PC-pois often shows a low Precision (Fig. 1; Supplementary Tables S1 and S2). This result is expected since the node conditional Poisson distributions are unable to model the over-dispersion generated by the (zero-inflated) negative binomial distributions.

On the other end of the spectrum, the more general zinb models work well in all scenarios (Fig. 1; Supplementary Tables S1 – S3). This is not surprising as the data are generated according to models (e.g. Poisson, NB) that can be seen as special cases of the zinb distribution, which means that in all tested scenarios the zinb model is correctly specified.

The PC-nb algorithm, based on the negative binomial assumption, performs reasonably well (Fig. 1; Supplementary Tables S1 – S3). However, in the hub graph (middle row of Fig. 1), its performances are slightly worse than the zinb models, showing low Precision when the true data generating distribution is node conditional zinb (Fig. 1; S1). This result indicates that a zero inflated negative binomial model may be needed when the mean is large (Risso *and others*, 2018).

As we expected from the considerations reported in Section 5, the performances of the variants of PC-zinb are quite similar to each other when the mean and the dispersion parameter are both

small, i.e., when the data are characterized by low mean and high variance ( $\mu = 0.5, \theta = 0.5$ ; Fig. 2; Supplementary Tables S1 – S3). This might be explained by the fact that a suitable choice of the parameters may allow non-zero inflated models to absorb the excess of zeros (see Section 5 for more details). Therefore, when applying our approach on this type of data, one should use the simplest variant, (i.e., PC-pois) to leverage the better computational performance (see last column of S1 – S3).

Finally, we see no difference in the performance of the PC-zinb variants (PC-zinb1 and PC-zinb0). This is perhaps not surprising, as we simulated the same structure of the graph for both  $\mu$  and  $\pi$ . These results suggest that the information inferred from  $\mu$  is sufficient to reconstruct the correct graph in this case.

We have focused here on  $p = 100$ , as this setting is closer to our real application. The results for  $p = 10$  are reported in Supplementary Figures S1 and S2 and Supplementary Tables S4–S6 and lead to similar conclusions.

## 7. RESULTS ON REAL DATA

We demonstrate our method on the motivating example dataset described in Section 2. Our analysis focuses on the total set of 1543 known transcription factors in mouse, which are thought to regulate the observed differentiation processes. We furthermore focus on the differentiation path starting at the activated HBC (HBC\*) stage (i.e., activated stem cells upon injury) up to mature neurons, therefore investigating the entire neuronal lineage in the trajectory of this dataset. As previously discussed in Section 2, we expect four different cell types along this path, being respectively HBC\*, GBC, iOSN and mOSN, and we estimate the structure of the graph for each of these cell types.

The average degree of the graphs is highest at the activated stem cell stage, with an average degree of 4, and decreases as cells develop to mature neurons, with average degrees of 3.9, 3.3 and 3.5 for the GBC, iOSN and mOSN networks, respectively. To interpret the graph structure, we focus on the 2-core of each network, i.e., we retain TFs that are associated with at least two other TFs, a preprocessing step that helps in understanding the core structure (Wang and Rohe, 2016).

We identify communities in each graph using the Leiden algorithm (Traag *and others*, 2019) and, in order to validate the associations discovered by PC-zinb, we interpret each of the communities by computing overlap with known functional gene sets in the MSigDB database (Subramanian *and others*, 2005; Liberzon *and others*, 2015), see Supplementary Material Section 2 for details. The interpretation of these communities relies on known processes involved in the development of the olfactory epithelium as found by previous research (e.g., Fletcher *and others* (2017); Gadye *and others* (2017)).

In the HBC\* cell type cluster, cells have been injured  $\sim 24$ h ago, so we expect response to injury, and stem cells actively preparing for differentiation, as well as replication to produce more stem cells to repair the epithelium. Four communities are discovered in the association network (Figure 3), broadly involved in either cell cycle, epigenetic mechanisms and (epithelial) cell differentiation (Supplementary Table S8). These communities reflect the need to divide in order to produce more cells, epigenetic mechanisms that are likely required to activate molecular processes upon injury, and the differentiation of stem cells to restore the damaged epithelium.

In the GBC cell type, we expect cells to proliferate to produce immature neurons. We discover four communities (Figure 3), broadly involved in DNA replication, cell proliferation, signaling, expression regulation and cell differentiation (Supplementary Table S9). Relevant pathways, such

as the P53 and notch signaling pathways, are also recovered for specific communities, and have previously been found to be involved in neurogenesis in neuroepithelial stem cells (Marin Navarro *and others*, 2020; Wang *and others*, 2011).

In the immature olfactory sensory neuron (iOSN) stage, we expect basal cells to start developing into immature neurons. Four communities are discovered (Figure 3), of which one community comprises the majority of the graph, i.e., 63% of all TFs retained in the graph, and importantly is involved in neurogenesis (Supplementary Table S10). Other, smaller, communities are enriched in processes such as cell and axon growth, wound healing, signaling and cell population maintenance.

Finally, in the mature olfactory sensory neuron stage (mOSN), we expect the final differentiation to functional neurons. Five communities are discovered (Figure 3), again with very different sizes. The largest communities are enriched in broader processes related to chromatin organization and transcription, possibly reflecting the basic changes required for cells to develop into and maintain at the mature stage (Supplementary Table S11). The third largest community is enriched specifically in the TGF-Beta pathway, known to be required for neurogenesis, and to modulate inflammatory responses (Meyers and Kessler, 2017).

Taken together, these results confirm previously known processes associated with differentiation of HBCs into mature neurons upon injury, with relevant processes highlighted by communities of transcription factors. Furthermore, while the community detection results are useful to validate the estimated graphs, they also provide a gateway to more detailed analysis, e.g., investigation of hub genes (e.g., Chen *and others* (2018)) or master regulators of development (e.g., Sikdar and Datta (2017)), therefore unlocking powerful interpretation of single-cell RNA-seq datasets.

## 8. DISCUSSION

In this work, we have introduced PC-zinb, a class of constraint-based algorithms for structure learning, supporting possibly overdispersed and zero-inflated count data. In focusing on these two nonstandard but realistic situations, our framework goes beyond what has so far been proposed in the literature. Moreover, by leveraging the proposal in Nguyen and Chiogna (2018) – shown to be competitive with state-of-the-art methods supporting count data – we inherit the benefits of that approach, most notably: the existence of a theoretical proof of convergence of the algorithm under suitable assumptions; an easy implementation of sparsity by a control on the number of variables in the conditional sets; invariance to feature scaling. On the synthetic datasets considered in Section 6, we showed that the algorithms work well in terms of reconstructing the structure from given data for large enough sample sizes, while providing biologically coherent information and insight on the real dataset analyzed in Section 7.

Our simulation studies allow us to derive various recommendations on the use of PC-zinb. Clearly, these do not rule out sensitivity analyses with respect to both model specification and tuning of the algorithms, which remain an important part of the model criticism process. A control of the level of significance of the tests with respect to the sample size,  $n$ , and the expected size of the neighborhood of each node,  $b$ , is highly recommended to guarantee good reconstruction abilities. As in real applications knowledge of the expected size of the neighborhood might be difficult to elicit, it may be prudent to try a range of values for  $b$ , and check stability of results. This might also generate a sequence of models of decreasing complexity for increasing values of  $b$  and whose dynamic might also point researchers to the most significant connections.

If only the structure of the graph is of interest, irrespective of the strength of the links among variables, we suggest making use of the Poisson variant of the algorithm when the mean of the variables is small, so as to reduce computational complexity. Moreover, when the mean of

the variables is small, presence of zero-inflation might not influence reconstruction abilities of the algorithms, as also confirmed by the small study on zero-inflation in Section 5. In these situations, we recommend using, at least in the first instance, non zero-inflated models.

If the null hypothesis  $H_0 : \beta_{st|K}^\mu = \beta_{st|K}^\pi = 0$  fails to be rejected, PC-zinb will remove the edge between variables  $s$  and  $t$ . While such a procedure can only be justified in settings with high power, our simulation study shows that, even in settings with small sample sizes, our algorithm is able to achieve high power, and the correct underlying structure of the graph can be learned successfully.

Our real data analysis, aimed at assessing biological validity of the reconstructed network, has demonstrated the great importance of finding meaningful visualizations of large complex networks. Our proposal, based on a search for communities of variables and their association to gene ontologies via enrichment analysis, allowed us to confirm both biological interpretability of the estimated structure, and to contribute to our understanding of which and where biological processes are occurring.

## 9. SOFTWARE

The methods presented in this article are available in the *learn2count* R package, available at <https://github.com/drisso/learn2count>. The code to reproduce the analyses of this paper is available at [https://github.com/drisso/structure\\_learning](https://github.com/drisso/structure_learning).

## 10. SUPPLEMENTARY MATERIAL

Supplementary material includes proofs and mathematical details, details on the real data analysis, and supplementary figures and tables.

## ACKNOWLEDGMENTS

The authors would like to thank Diya Das, Rebecca Chance, and John Ngai for providing access to the data and for help with the biological interpretation of the results.

DR was supported by “Programma per Giovani Ricercatori Rita Levi Montalcini” granted by the Italian Ministry of Education and University Research. NTKH was supported by the project of excellence “Statistical methods and models for complex data” awarded to the Department of Statistical Sciences, University of Padova by the Italian Ministry for Education and University Research. KVDB is a postdoctoral fellow of the Belgian American Educational Foundation (BAEF) and is supported by the Research Foundation Flanders (FWO), grant 1246220N.

*Conflict of Interest:* None declared.

## REFERENCES

- ABEGAZ, F. AND WIT, E. (2015). Copula gaussian graphical models with penalized ascent monte carlo em algorithm. *Statistica Neerlandica* **69**(4), 419–441.
- ALLEN, G. AND LIU, Z. (2013). A local Poisson graphical model for inferring networks from sequencing data. *IEEE Transactions on Nanobioscience* **12**(3), 189–198.
- BESAG, J. (1974). Spatial interaction and the statistical analysis of lattice systems. *Journal of*

- the Royal Statistical Society. Series B (Methodological)* **36**(2), 192–236.
- BRANN, D. H., TSUKAHARA, T., WEINREB, C., LIPOVSEK, M., VAN DEN BERGE, K., GONG, B., CHANCE, R., MACAULAY, I. C., CHOU, H. J., FLETCHER, R. B. *and others.* (2020). Non-neuronal expression of sars-cov-2 entry genes in the olfactory system suggests mechanisms underlying covid-19-associated anosmia. *Science Advances* **6**(31), eabc5801.
- BRYAN, A. H. (2020). *HiveR: 2D and 3D Hive Plots for R*. R package version 0.3.63.
- CHEN, D., YAN, W., FU, L. Y. AND KAUFMANN, K. (2018, dec). Architecture of gene regulatory networks controlling flower development in *Arabidopsis thaliana*. *Nature Communications* **9**(1), 4534.
- COLOMBO, D. AND MAATHUIS, M. H. (2014). Order-independent constraint-based causal structure learning. *Journal of Machine Learning Research* **15**(1), 3741–3782.
- CSARDI, G., NEPUSZ, T. *and others.* (2006). The igraph software package for complex network research. *InterJournal, complex systems* **1695**(5), 1–9.
- DRTON, M. AND MAATHUIS, M. H. (2017). Structure learning in graphical modeling. *Annual Review of Statistics and Its Application* **4**(1), 365–393.
- FLETCHER, R. B., DAS, D., GADYE, L., STREET, K. N., BAUDHUIN, A., WAGNER, A., COLE, M. B., FLORES, Q., CHOI, Y. G., YOSEF, N. *and others.* (2017). Deconstructing olfactory stem cell trajectories at single-cell resolution. *Cell Stem Cell* **20**(6), 817–830.
- GADYE, L., DAS, D., SANCHEZ, M. A., STREET, K., BAUDHUIN, A., WAGNER, A., COLE, M. B., CHOI, Y. G., YOSEF, N., PURDOM, E. *and others.* (2017). Injury activates transient olfactory stem cell states with diverse lineage capacities. *Cell Stem Cell* **21**(6), 775–790.
- GALLOPIN, M., RAU, A. AND JAFFRÉZIC, F. (2013). A hierarchical Poisson log-normal model for network inference from RNA sequencing data. *PloS One* **8**(10), e77503.
- IRIZARRY, R. A., HOBBS, B., COLLIN, F., BEAZER-BARCLAY, Y. D., ANTONELLIS, K. J., SCHERF, U. AND SPEED, T. P. (2003). Exploration, normalization, and summaries of high density oligonucleotide array probe level data. *Biostatistics* **4**(2), 249–264.
- ISLAM, S., ZEISEL, A., JOOST, S., LA MANNO, G., ZAJAC, P., KASPER, M., LÖNNERBERG, P. AND LINNARSSON, S. (2014). Quantitative single-cell rna-seq with unique molecular identifiers. *Nature Methods* **11**(2), 163.
- JUNBAI, W., LEO, W. K. C. AND JAN, D. (2005). New probabilistic graphical models for genetic regulatory networks studies. *Journal of Biomedical Informatics* **38**(6), 443 – 455.
- KOŁODZIEJCZYK, A. A., KIM, J. K., SVENSSON, V., MARIONI, J. C. AND TEICHMANN, S. A. (2015). The technology and biology of single-cell rna sequencing. *Molecular cell* **58**(4), 610–620.
- KRZYWINSKI, M., BIROL, I., JONES, S. JM AND MARRA, M. A. (2012). Hive plots—rational approach to visualizing networks. *Briefings in Bioinformatics* **13**(5), 627–644.
- LAURITZEN, S. L. (1996). *Graphical Models*, Volume 17. Clarendon Press, Oxford.

- LIBERZON, A., BIRGER, C., THORVALDSDÓTTIR, H., GHANDI, M., MESIROV, J. P. AND TAMAYO, P. (2015, dec). The Molecular Signatures Database Hallmark Gene Set Collection. *Cell Systems* **1**(6), 417–425.
- LIU, H., ROEDER, K. AND WASSERMAN, L. (2010). Stability approach to regularization selection (stars) for high dimensional graphical models. In: *Advances in neural information processing systems*. pp. 1432–1440.
- MACOSKO, E. Z., BASU, A., SATIJA, R., NEMESH, J., SHEKHAR, K., GOLDMAN, M., TIROSH, I., BIALAS, A. R., KAMITAKI, N., MARTERSTECK, E. M. *and others*. (2015). Highly parallel genome-wide expression profiling of individual cells using nanoliter droplets. *Cell* **161**(5), 1202–1214.
- MARIN NAVARRO, A., PRONK, R. J., VAN DER GEEST, A. T., OLIYNYK, G., NORDGREN, A., ARSENIAN-HENRIKSSON, M., FALK, A. AND WILHELM, M. (2020, jan). p53 controls genomic stability and temporal differentiation of human neural stem cells and affects neural organization in human brain organoids. *Cell Death & Disease* **11**(1), 52.
- MCDAVID, A., GOTTARDO, R., SIMON, N. AND DRTON, M. (2019). Graphical models for zero-inflated single cell gene expression. *The Annals of Applied Statistics* **13**(2), 848.
- MEYERS, E. A. AND KESSLER, J. A. (2017, aug). TGF- $\beta$  Family Signaling in Neural and Neuronal Differentiation, Development, and Function. *Cold Spring Harbor perspectives in biology* **9**(8), a022244.
- NGUYEN, T. K. H. AND CHIOGNA, M. (2018). Structure learning of undirected graphical models for count data. *ArXiv*, 1810.10854.
- PEÑA, J. M. (2008). Learning gaussian graphical models of gene networks with false discovery rate control. In: Marchiori E., Moore J.H. (editor), *Evolutionary Computation, Machine Learning and Data Mining in Bioinformatics.*, Volume 4973, Lecture Notes in Computer Science. Springer.
- PICELLI, S., FARIDANI, O. R., BJÖRKLUND, Å. K., WINBERG, G., SAGASSER, S. AND SANDBERG, R. (2014). Full-length rna-seq from single cells using smart-seq2. *Nature Protocols* **9**(1), 171.
- RISSO, D., PERRAUDEAU, F., GRIBKOVA, S., DUDOIT, S. AND VERT, J. P. (2018). A general and flexible method for signal extraction from single-cell rna-seq data. *Nature Communications* **9**(1), 1–17.
- SCHÄFER, J. AND STRIMMER, K. (2005). An empirical bayes approach to inferring large-scale gene association networks. *Bioinformatics* **21**(6), 754–764.
- SIKDAR, S. AND DATTA, S. (2017, dec). A novel statistical approach for identification of the master regulator transcription factor. *BMC Bioinformatics* **18**(1), 79.
- SPIRITES, P., GLYMOUR, C. N. AND SCHEINES, R. (2000). *Causation, prediction, and search*. MIT press.
- SUBRAMANIAN, A., TAMAYO, P., MOOTHA, V. K., MUKHERJEE, S., EBERT, B. L., GILLETTE, M. A., PAULOVICH, A., POMEROY, S. L., GOLUB, T. R., LANDER, E. S. *and others*. (2005). Gene set enrichment analysis: A knowledge-based approach for interpreting genome-wide expression profiles. *Proceedings of the National Academy of Sciences* **102**(43), 15545–15550.

- SVENSSON, V. (2020). Droplet scrna-seq is not zero-inflated. *Nature Biotechnology* **38**(2), 1–4.
- TOWNES, F. W., HICKS, S. C., ARYEE, M. J. AND IRIZARRY, R. A. (2019). Feature selection and dimension reduction for single-cell rna-seq based on a multinomial model. *Genome Biology* **20**(1), 1–16.
- TRAAG, V. A., WALTMAN, L. AND VAN ECK, N. J. (2019). From Louvain to Leiden: guaranteeing well-connected communities. *Scientific Reports* **9**(1), 5233.
- VAN DE WIEL, M. A., LEDAY, G. G., PARDO, L., RUE, H., VAN DER VAART, A. W. AND VAN WIERINGEN, W. N. (2013). Bayesian analysis of rna sequencing data by estimating multiple shrinkage priors. *Biostatistics* **14**(1), 113–128.
- VIETH, B., ZIEGENHAIN, C., PAREKH, S., ENARD, W. AND HELLMANN, I. (2017). powsimr: power analysis for bulk and single cell rna-seq experiments. *Bioinformatics* **33**(21), 3486–3488.
- WANG, S. AND ROHE, K. (2016, 12). Discussion of “coauthorship and citation networks for statisticians”. *Ann. Appl. Stat.* **10**(4), 1820–1826.
- WANG, W., LIU, W., WANG, Y., ZHOU, L., TANG, X. AND LUO, H. (2011, feb). Notch signaling regulates neuroepithelial stem cell maintenance and neuroblast formation in Drosophila optic lobe development. *Developmental Biology* **350**(2), 414–428.
- WANG, Z., GERSTEIN, M. AND SNYDER, M. (2009). RNA-Seq: a revolutionary tool for transcriptomics. *Nature Reviews Genetics* **10**(1), 57–63.
- YANG, E., RAVIKUMAR, P. K., ALLEN, G. I. AND LIU, Z. (2013). On poisson graphical models. In: *Advances in neural information processing systems*. pp. 1718–1726.
- YANG, E., RAVIKUMAR, P. K., ALLEN, G. I. AND LIU, Z. (2015). Graphical models via univariate exponential family distributions. *Journal of Machine Learning Research* **16**(115), 3813–3847.
- YIN, J. AND LI, H. (2011). A sparse conditional gaussian graphical model for analysis of genetical genomics data. *The annals of applied statistics* **5**(4), 2630.
- ZHENG, G. XY, TERRY, J. M., BELGRADER, P., RYVKIN, P., BENT, Z. W., WILSON, R., ZIRALDO, S. B., WHEELER, T. D., MCDERMOTT, G. P., ZHU, J. and others. (2017). Massively parallel digital transcriptional profiling of single cells. *Nature Communications* **8**(1), 1–12.

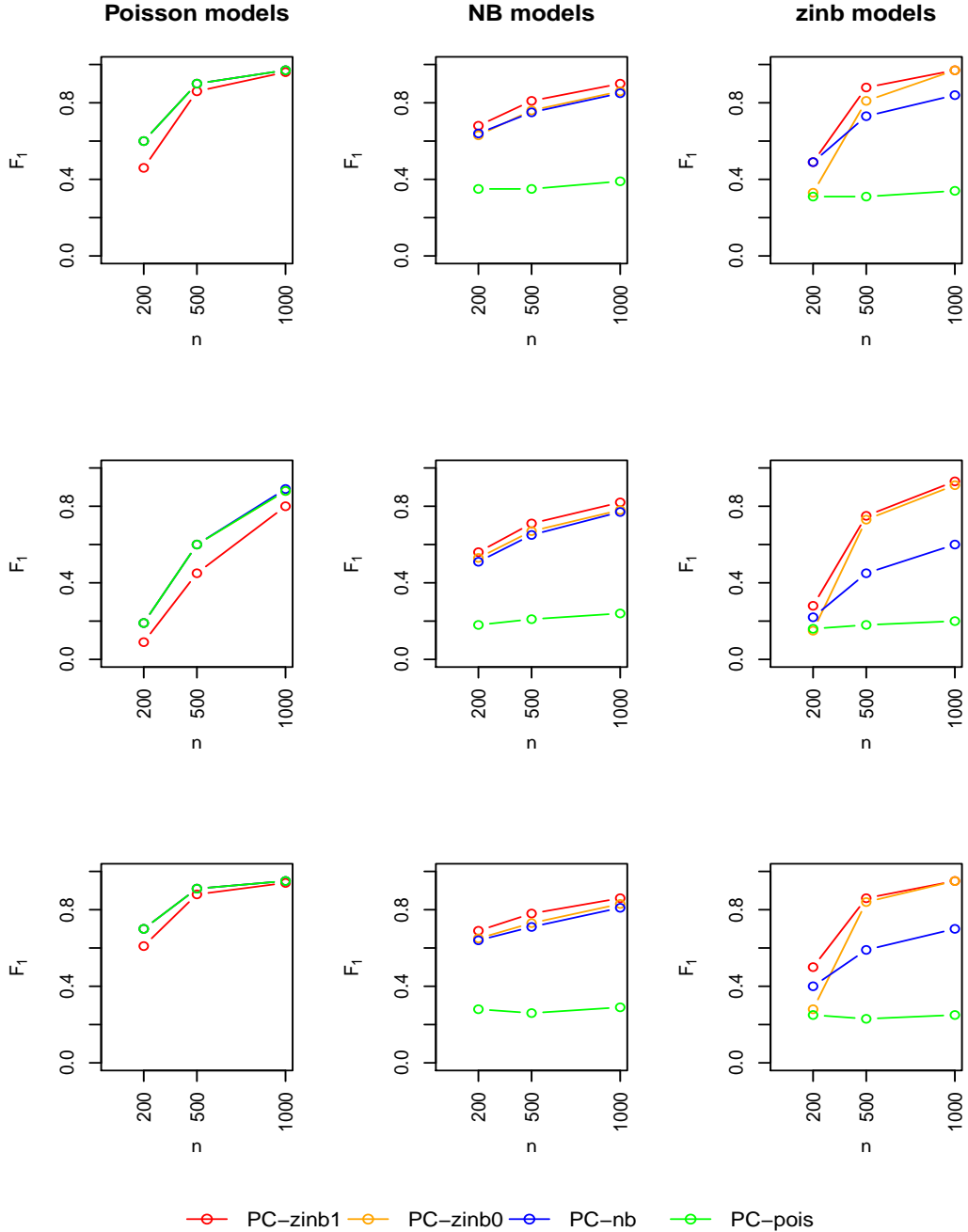


Fig. 1:  $F_1$ -score of the considered algorithms for the three types of graphs in Supplementary Figure S2 with  $p = 100, \mu = 5, \theta = 0.5, \pi = 0.7$ : random (top); hub (middle); scale-free (bottom). The data were simulated from Poisson (left), NB (middle), and zinb (right) models. PC-zinb1: zinb model in which the structure of the graph is attributable to both of the two parameter components  $\mu_{s|K}$  and  $\pi_{s|K}$ ; PC-zinb0: zinb model in which the structure of the graph is attributable to only the parameter component  $\mu_{s|K}$  and consider  $\pi_{s|K}$  as a constant; PC-nb: Negative binomial model, i.e., the special case of zinb models where  $\pi_{s|K} = 0$ ; PC-pois: Poisson model of Nguyen and Chiogna (2018).



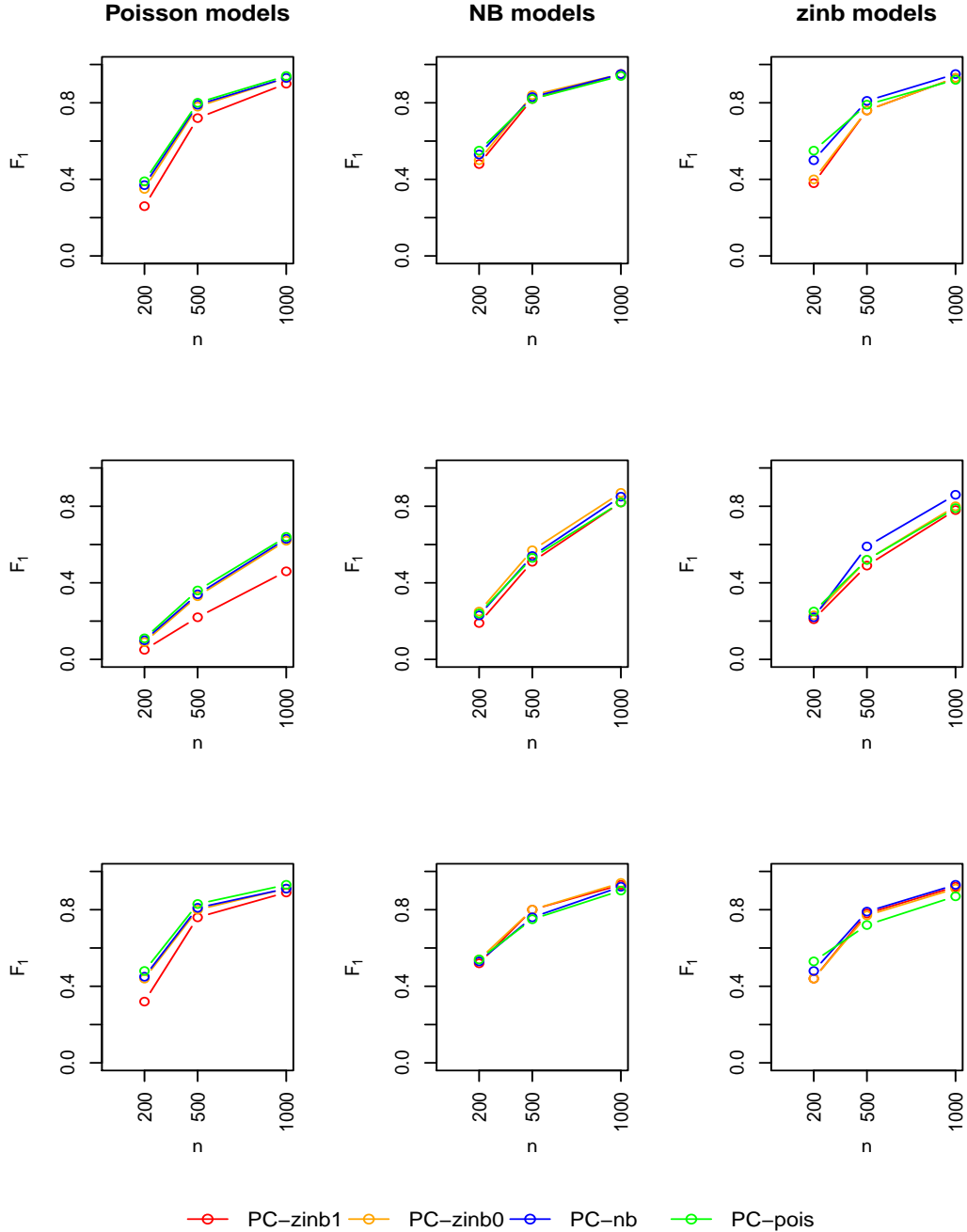


Fig. 2:  $F_1$ -score of the considered algorithms for the three types of graphs in Supplementary Figure S2 with  $p = 100$ ,  $\mu = 0.5$ ,  $\theta = 0.5$ ,  $\pi = 0.7$ : random (top); hub (middle); scale-free (bottom). The data were simulated from Poisson (left), NB (middle), and zinb (right) models. PC-zinb1: zinb model in which the structure of the graph is attributable to both of the two parameter components  $\mu_{s|K}$  and  $\pi_{s|K}$ ; PC-zinb0: zinb model in which the structure of the graph is attributable to only the parameter component  $\mu_{s|K}$  and consider  $\pi_{s|K}$  as a constant; PC-nb: Negative binomial model, i.e., the special case of zinb models where  $\pi_{s|K} = 0$ ; PC-pois: Poisson model of Nguyen and Chiogna (2018).

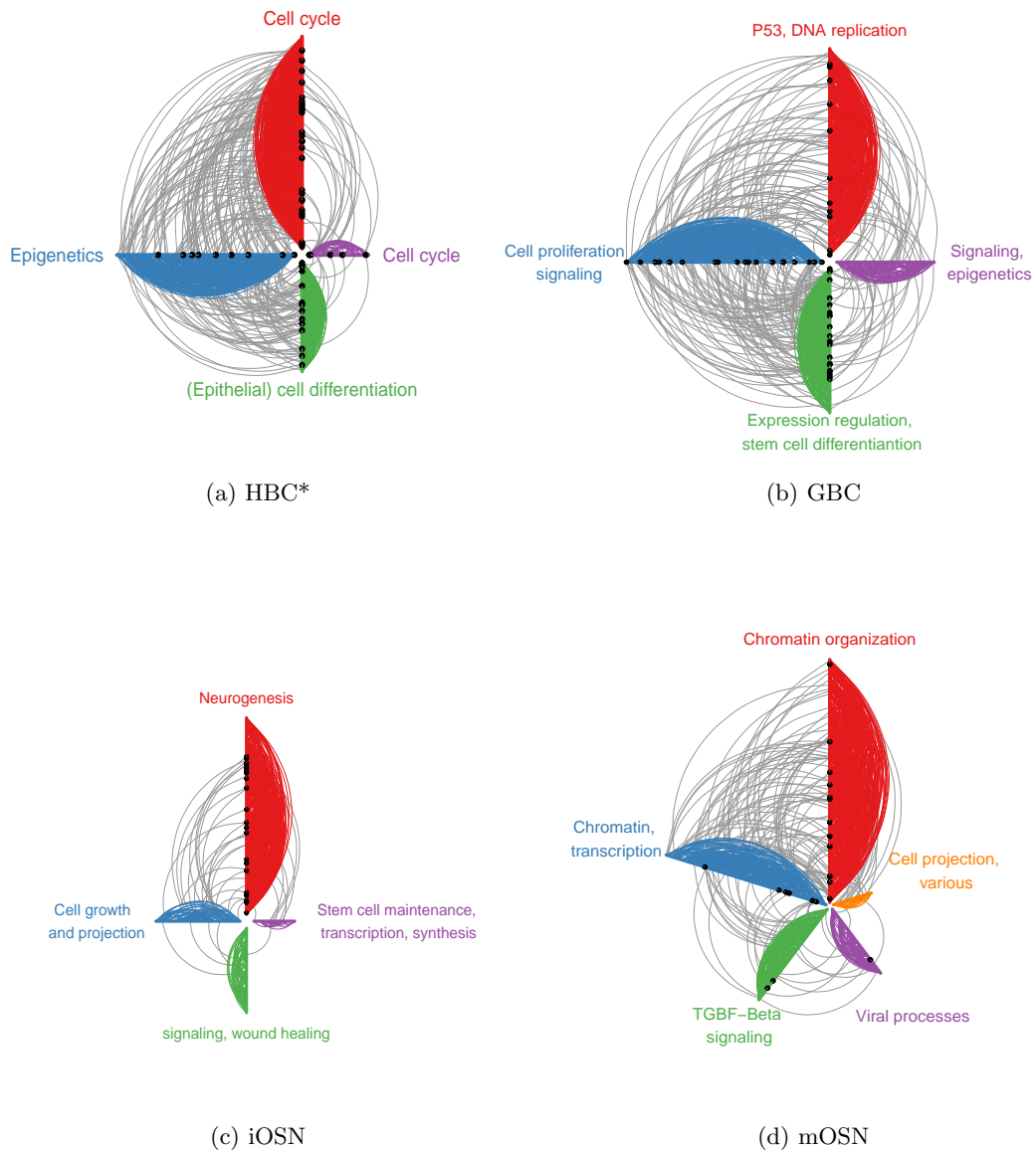


Fig. 3: Hive plots (Krzywinski *and others*, 2012; Bryan, 2020) of TF gene networks estimated with PC-zinb. Gene communities were estimated using the Leiden algorithm and are represented on the axes of the plots and by different edge colors; hub nodes are represented as solid black circles. Each axis (community) was annotated with the most enriched gene set (see Supplementary Material Section 2).

Table 1: Hellinger distance between zinb and NB distribution

$\theta_0$	$\mu_0$	$\pi$									
		0	0.1	0.2	0.3	0.4	0.5	0.6	0.7	0.8	0.9
0.5	0.5	0.00	0.02	0.05	0.07	0.10	0.13	0.16	0.19	0.23	0.28
	5	0.00	0.05	0.10	0.15	0.20	0.25	0.30	0.36	0.42	0.50
	10	0.00	0.06	0.12	0.18	0.23	0.29	0.34	0.40	0.47	0.55
	15	0.00	0.07	0.13	0.19	0.25	0.31	0.37	0.43	0.50	0.58
	20	0.00	0.07	0.14	0.20	0.26	0.32	0.38	0.44	0.51	0.60
	25	0.00	0.08	0.15	0.21	0.27	0.33	0.39	0.46	0.52	0.61
5	0.5	0.00	0.03	0.06	0.09	0.12	0.15	0.19	0.23	0.27	0.33
	5	0.00	0.13	0.22	0.30	0.37	0.43	0.50	0.57	0.64	0.72
	10	0.00	0.19	0.28	0.36	0.43	0.50	0.57	0.63	0.70	0.79
	15	0.00	0.21	0.30	0.38	0.45	0.52	0.59	0.65	0.72	0.81
	20	0.00	0.21	0.31	0.39	0.46	0.53	0.59	0.66	0.73	0.82
	25	0.00	0.22	0.32	0.40	0.47	0.53	0.60	0.67	0.74	0.82

# Supplementary material to Structure learning for zero-inflated counts, with an application to single-cell RNA sequencing data

NGUYEN THI KIM HUE

*Department of Statistical Sciences, University of Padova, Padova, Italy.*

KOEN VAN DEN BERGE

*Department of Statistics, University of California, Berkeley, Berkeley, CA, USA.  
Department of Applied Mathematics, Computer Science and Statistics, Ghent University,  
Ghent, Belgium.*

MONICA CHIOGNA

*Department of Statistical Sciences, University of Bologna, Italy.*

DAVIDE RISSO\*

*Department of Statistical Sciences, University of Padova, Padova, Italy.  
davide.risso@unipd.it*

## 1. PROOFS AND MATHEMATICAL DETAILS

In Section 1.1, we provide the proof of Theorem 3.1 (Section 3 of main paper); Section 1.2 describes the maximum likelihood estimation procedure used in zinb regressions; in Section 1.3 we prove the identifiability of zinb models (Section 3 of main paper).

### 1.1 Proof of Theorem 3.1

In what follows, we will first consider the case  $K = V$ . Results for general case  $K \subseteq V$  will be then deduced.

We note that the set of explanatory variables  $\mathbf{X}_{K \setminus \{s\}}$  in the generalized linear model  $X_s$  given  $\mathbf{X}_{K \setminus \{s\}}$  does not include variable  $X_t$ , with  $t \in V \setminus K$ . Suppose we zero-pad the true parameter  $\beta_{s|K} \in \mathbb{R}^{2^{|K|}-2}$  to include zero weights over  $V \setminus K$ , then the resulting parameter would lie in  $\mathbb{R}^{2^{|p|-1}}$ . To simplify notation, we write  $(\mu_j, \pi_j, \beta_{jk}^\mu, \beta_{jk}^\pi)$  instead of  $(\mu_{j|V}, \pi_{j|V}, \beta_{jk|V}^\mu, \beta_{jk|V}^\pi)$ .

*Proof.* It is easy to show that for  $\mathbf{x} = (x_1, x_2, \dots, x_p)$  and  $\mathbf{y} = (y_1, y_2, \dots, y_p)$  one can write

$$\frac{P(\mathbf{x})}{P(\mathbf{y})} = \prod_{j=1}^p \frac{P(x_j | x_1, \dots, x_{j-1}, y_{j+1}, \dots, y_p)}{P(y_j | x_1, \dots, x_{j-1}, y_{j+1}, \dots, y_p)}.$$

Let  $\mathbf{y} = (0, 0, \dots, 0)$ . It holds

$$\begin{aligned} \frac{P(\mathbf{x})}{P(\mathbf{0})} &= \prod_{j=1}^p \frac{P(x_j | x_1, \dots, x_{j-1}, 0, \dots, 0)}{P(0 | x_1, \dots, x_{j-1}, 0, \dots, 0)} \\ &= \prod_{j=1}^p \frac{\pi_j^0 \delta_0(x_j) + (1 - \pi_j^0) f_{NB}(x_j, \mu_j^0, \theta_j)}{\pi_j^0 + (1 - \pi_j^0) f_{NB}(0, \mu_j^0, \theta_j)}, \end{aligned} \quad (1.1)$$

where  $\mu_j^0 = \exp\{\beta_j^\mu + \sum_{k=1}^{j-1} \beta_{jk}^\mu x_k\}$ , and  $\text{logit}(1 - \pi_j^0) = \beta_j^\pi + \sum_{k=1}^{j-1} \beta_{jk}^\pi x_k$ . Consider the following two cases.

- $\beta_{jk}^\mu \leq 0, \forall j, k \in V$ .

Here,  $\mu_j^0 \rightarrow 0$  when  $\|\mathbf{x}\|_\infty \rightarrow \infty$ . From Equation 1.1, one has

$$\begin{aligned} \frac{P(\mathbf{x})}{P(\mathbf{0})} &= \prod_{j=1}^p \left( \frac{\pi_j^0 \delta_0(x_j) + (1 - \pi_j^0) f_{NB}(x_j, \mu_j^0, \theta_j)}{\pi_j^0 + (1 - \pi_j^0) f_{NB}(0, \mu_j^0, \theta_j)} \right) \\ &\leq \prod_{j=1}^p \left( \delta_0(x_j) + \frac{f_{NB}(x_j, \mu_j^0, \theta_j)}{f_{NB}(0, \mu_j^0, \theta_j)} \right) \\ &= \prod_{j=1}^p \delta_0(x_j) + \sum_{j=1}^p \frac{f_{NB}(x_j, \mu_j^0, \theta_j)}{f_{NB}(0, \mu_j^0, \theta_j)} \prod_{k \in V \setminus \{j\}} \delta_0(x_k) \\ &\quad + \sum_{i < j} \frac{f_{NB}(x_i, \mu_i^0, \theta_i)}{f_{NB}(0, \mu_i^0, \theta_i)} \frac{f_{NB}(x_j, \mu_j^0, \theta_j)}{f_{NB}(0, \mu_j^0, \theta_j)} \prod_{k \in V \setminus \{i, j\}} \delta_0(x_k) \\ &\quad + \sum_{i < j < k} \frac{f_{NB}(x_i, \mu_i^0, \theta_i)}{f_{NB}(0, \mu_i^0, \theta_i)} \frac{f_{NB}(x_j, \mu_j^0, \theta_j)}{f_{NB}(0, \mu_j^0, \theta_j)} \frac{f_{NB}(x_k, \mu_k^0, \theta_k)}{f_{NB}(0, \mu_k^0, \theta_k)} \prod_{t \in V \setminus \{i, j, k\}} \delta_0(x_t) \\ &\quad + \dots + \prod_{j=1}^p \frac{f_{NB}(x_j, \mu_j^0, \theta_j)}{f_{NB}(0, \mu_j^0, \theta_j)}. \end{aligned}$$

To prove existence of the joint distribution, it is sufficient to control the term

$$\prod_{j=1}^p \left( \delta_0(x_j) + \frac{f_{NB}(x_j, \mu_j^0, \theta_j)}{f_{NB}(0, \mu_j^0, \theta_j)} \right).$$

Indeed, taking the sum over  $x_1, x_2, \dots, x_p$ , one gets

$$\begin{aligned}
& \sum_{x_1, \dots, x_p} \prod_{j=1}^p \left( \delta_0(x_j) + \frac{f_{NB}(x_j, \mu_j^0, \theta_j)}{f_{NB}(0, \mu_j^0, \theta_j)} \right) \\
&= 1 + \sum_{j=1}^p \frac{1}{f_{NB}(0, \mu_j^*, \theta_j)} \\
&+ \sum_{i < j} \sum_{x_i, x_j} \frac{f_{NB}(x_i, \mu_i^*, \theta_i)}{f_{NB}(0, \mu_i^*, \theta_i)} \frac{f_{NB}(x_j, \mu_j^i, \theta_j)}{f_{NB}(0, \mu_j^i, \theta_j)} \\
&+ \sum_{i < j < k} \sum_{x_i, x_j, x_k} \frac{f_{NB}(x_i, \mu_i^*, \theta_i)}{f_{NB}(0, \mu_i^*, \theta_i)} \frac{f_{NB}(x_j, \mu_j^i, \theta_j)}{f_{NB}(0, \mu_j^i, \theta_j)} \frac{f_{NB}(x_k, \mu_k^{i,j}, \theta_k)}{f_{NB}(0, \mu_k^{i,j}, \theta_k)} \\
&+ \dots + \sum_{x_1, \dots, x_p} \frac{f_{NB}(x_j, \mu_j^0, \theta_j)}{f_{NB}(0, \mu_j^0, \theta_j)},
\end{aligned} \tag{1.2}$$

where  $\mu_i^* = \exp\{\beta_i^\mu\}$ ,  $\mu_j^i = \exp\{\beta_j^\mu + \beta_{ji}^\mu x_i\}$ ,  $\mu_k^{i,j} = \exp\{\beta_k^\mu + \beta_{ki}^\mu x_i + \beta_{kj}^\mu x_j\}$ ; and  $\text{logit}(1 - \pi_i^*) = \beta_i^\pi$ ,  $\text{logit}(1 - \pi_j^i) = \beta_j^\pi + \beta_{ji}^\pi x_i$ , and  $\text{logit}(1 - \pi_k^{i,j}) = \beta_k^\pi + \beta_{ki}^\pi x_i + \beta_{kj}^\pi x_j$ . Moreover, for  $x_j$  large enough

$$\begin{aligned}
\frac{f_{NB}(x_j, \mu_j^0, \theta_j)}{f_{NB}(0, \mu_j^0, \theta_j)} &= \frac{\Gamma(x_j + \theta_j)}{\Gamma(x_j + 1)\Gamma(\theta_j)} \left( \frac{\mu_j^0}{\theta_j + \mu_j^0} \right)^{x_j} \\
&= O \left( x_j^{\theta_j - 1} \left( \frac{\mu_j^0}{\theta_j + \mu_j^0} \right)^{x_j} \right) \\
&= O \left( \left( \frac{\mu_j^0}{\theta_j + \mu_j^0} \right)^{x_j} \right) \\
&\leq O(q^{x_j}),
\end{aligned}$$

for some  $q < 1$ . Therefore, when  $x_j$  is large enough, from Equation 1.2, one has

$$\begin{aligned}
\sum_{x_1, \dots, x_p} \prod_{j=1}^p \left( \delta_0(x_j) + \frac{f_{NB}(x_j, \mu_j^0, \theta_j)}{f_{NB}(0, \mu_j^0, \theta_j)} \right) &\leq c_o + \sum_{i < j} \sum_{x_i, x_j} O(q^{x_i}) O(q^{x_j}) \\
&+ \sum_{i < j < k} \sum_{x_i, x_j, x_k} O(q^{x_i}) O(q^{x_j}) O(q^{x_k}) \\
&+ \dots + \sum_{x_1, \dots, x_p} \prod_{j=1}^p O(q^{x_j}) \\
&\leq \infty,
\end{aligned}$$

that proves existence of the joint distribution.

- At least one parameter  $\beta_{jk}^\mu > 0$ .

Without loss of generality, one can assume  $\beta_{p(p-1)}^\mu > 0$ . Then,  $\mu_p^{p-1} \rightarrow \infty$ , when  $x_{p-1} \rightarrow \infty$ . From Equation 1.1, one has

$$\begin{aligned} \frac{P(\mathbf{x})}{P(\mathbf{0})} &= \prod_{j=1}^p \frac{\pi_j \delta_0(x_j) + (1 - \pi_j) f_{NB}(x_j, \mu_j^0, \theta_j)}{\pi_j + (1 - \pi_j) f_{NB}(0, \mu_j^0, \theta_j)} \\ &\geq \prod_{j=1}^p (\pi_j \delta_0(x_j) + (1 - \pi_j) f_{NB}(x_j, \mu_j^0, \theta_j)), \end{aligned}$$

Moreover,

$$\begin{aligned} &\prod_{j=1}^p (\pi_j \delta_0(x_j) + (1 - \pi_j) f_{NB}(x_j, \mu_j^0, \theta_j)) \\ &= \prod_{j=1}^p \pi_j \delta_0(x_j) + \sum_{j=1}^p (1 - \pi_j) f_{NB}(x_j, \mu_j^0, \theta_j) \prod_{k \in V \setminus \{j\}} \pi_k \delta_0(x_k) \\ &\quad + \sum_{i < j} (1 - \pi_i) f_{NB}(x_i, \mu_i^0, \theta_i) (1 - \pi_j) f_{NB}(x_j, \mu_j^0, \theta_j) \prod_{k \in V \setminus \{i, j\}} \pi_k \delta_0(x_k) \\ &\quad + \sum_{i < j < k} (1 - \pi_i) f_{NB}(x_i, \mu_i^0, \theta_i) (1 - \pi_j) f_{NB}(x_j, \mu_j^0, \theta_j) (1 - \pi_k) f_{NB}(x_k, \mu_k^0, \theta_k) \\ &\quad \prod_{t \in V \setminus \{i, j, k\}} \pi_t \delta_0(x_t) + \dots + \prod_{j=1}^p (1 - \pi_j) f_{NB}(x_j, \mu_j^0, \theta_j). \end{aligned}$$

Taking the sum over  $x_1, x_2, \dots, x_p$  of the term

$$(1 - \pi_{p-1}) f_{NB}(x_{p-1}, \mu_{p-1}^0, \theta_{p-1}) (1 - \pi_p) f_{NB}(x_p, \mu_p^0, \theta_p) \prod_{k \in V \setminus \{p-1, p\}} \pi_k \delta_0(x_k),$$

yields

$$\begin{aligned} &\sum_{x_1, \dots, x_p} (1 - \pi_{p-1}) f_{NB}(x_{p-1}, \mu_{p-1}^0, \theta_{p-1}) (1 - \pi_p) f_{NB}(x_p, \mu_p^0, \theta_p) \prod_{k \in V \setminus \{p-1, p\}} \pi_k \delta_0(x_k) \\ &= O \left( \sum_{x_{p-1}, x_p} (1 - \pi_{p-1}^*) f_{NB}(x_{p-1}, \mu_{p-1}^*, \theta_{p-1}) (1 - \pi_p^{p-1}) f_{NB}(x_p, \mu_p^{p-1}, \theta_p) \right) \\ &= O \left( \sum_{x_{p-1}, x_p} (1 - \pi_p^{p-1}) f_{NB}(x_{p-1}, \mu_{p-1}^*, \theta_{p-1}) f_{NB}(x_p, \mu_p^{p-1}, \theta_p) \right) \\ &= O \left( \sum_{x_{p-1}, x_p} (1 - \pi_p^{p-1}) \frac{\Gamma(x_{p-1} + \theta_{p-1})}{\Gamma(x_{p-1} + 1) \Gamma(\theta_{p-1})} \left( \frac{\theta_{p-1}}{\theta_{p-1} + \mu_{p-1}^*} \right)^{\theta_{p-1}} \left( \frac{\mu_{p-1}^*}{\theta_{p-1} + \mu_{p-1}^*} \right)^{x_{p-1}} \right. \\ &\quad \left. \frac{\Gamma(x_p + \theta_p)}{\Gamma(x_p + 1) \Gamma(\theta_p)} \left( \frac{\theta_p}{\theta_p + \mu_p^{p-1}} \right)^{\theta_p} \left( \frac{\mu_p^{p-1}}{\theta_p + \mu_p^{p-1}} \right)^{x_p} \right). \tag{1.3} \end{aligned}$$

– If  $\beta_{p(p-1)}^\pi > 0$ , then  $1 - \pi_p^{p-1} = \frac{\exp\{\beta_p^\pi + \beta_{p(p-1)}^\pi x_{p-1}\}}{1 + \exp\{\beta_p^\pi + \beta_{p(p-1)}^\pi x_{p-1}\}} \rightarrow 1$  when  $x_{p-1} \rightarrow \infty$ .

Let  $x_p = O(\mu_p^{p-1})$  be large enough. From Equation 1.3, one gets

$$\begin{aligned}
& \sum_{x_1, \dots, x_p} (1 - \pi_{p-1}) f_{NB}(x_{p-1}, \mu_{p-1}^0, \theta_{p-1}) (1 - \pi_p) f_{NB}(x_p, \mu_p^0, \theta_2) \prod_{k \in V \setminus \{p-1, p\}} \pi_k \delta_0(x_k) \\
&= \sum_{x_{p-1}, x_p} O \left( x_{p-1}^{\theta_{p-1}-1} \left( \frac{\mu_{p-1}^*}{\theta_{p-1} + \mu_{p-1}^*} \right)^{x_{p-1}} x_p^{\theta_p-1} \left( \frac{\theta_p}{\theta_p + \mu_p^{p-1}} \right)^{\theta_p} \exp \left( -\frac{\theta_p}{\mu_p^{p-1}} x_p \right) \right) \\
&= \sum_{x_{p-1}, x_p} O \left( \frac{1}{x_p} \left( \frac{\mu_{p-1}^*}{\theta_{p-1} + \mu_{p-1}^*} \right)^{x_{p-1}} \right) \\
&= \sum_{x_p} O \left( \frac{1}{x_p} \right) \\
&\rightarrow \infty.
\end{aligned}$$

– If  $\beta_{p(p-1)}^\pi < 0$ , then  $1 - \pi_p^{p-1} = \frac{\exp\{\beta_p^\pi + \beta_{p(p-1)}^\pi x_{p-1}\}}{1 + \exp\{\beta_p^\pi + \beta_{p(p-1)}^\pi x_{p-1}\}} = O(\exp\{\beta_{p(p-1)}^\pi x_{p-1}\})$ .

Let  $x_p = O(\mu_p^{p-1})$  be large enough. From Equation 1.3, one gets

$$\begin{aligned}
& \sum_{x_1, \dots, x_p} (1 - \pi_{p-1}) f_{NB}(x_{p-1}, \mu_{p-1}^0, \theta_{p-1}) (1 - \pi_p) f_{NB}(x_p, \mu_p^0, \theta_2) \prod_{k \in V \setminus \{p-1, p\}} \pi_k \delta_0(x_k) \\
&= \sum_{x_{p-1}, x_p} O \left( e^{\beta_{p(p-1)}^\pi x_{p-1}} x_{p-1}^{\theta_{p-1}-1} \left( \frac{\mu_{p-1}^*}{\theta_{p-1} + \mu_{p-1}^*} \right)^{x_{p-1}} x_p^{\theta_p-1} \left( \frac{\theta_p}{\theta_p + \mu_p^{p-1}} \right)^{\theta_p} \exp \left( -\frac{\theta_p}{\mu_p^{p-1}} x_p \right) \right) \\
&= \sum_{x_{p-1}, x_p} O \left( \frac{1}{x_p} \left( e^{\beta_{p(p-1)}^\pi} \frac{\mu_{p-1}^*}{\theta_{p-1} + \mu_{p-1}^*} \right)^{x_{p-1}} \right) \\
&= \sum_{x_p} O \left( \frac{1}{x_p} \right) \\
&\rightarrow \infty.
\end{aligned}$$

Therefore, the joint distribution exists if and only if all regression coefficients  $\beta_{st|K}^\mu$  are negative,  $\forall K \subseteq V$ .  $\square$

## 1.2 Numerical optimization of the likelihood function

Given a set of data  $\mathbb{X}$ , for each  $s \in K \subseteq V$ , we estimate parameters  $\boldsymbol{\nu}_{s|K}, \boldsymbol{\beta}_{s|K}, \theta_s$  by maximizing the local log-likelihood function

$$\ell_s(\boldsymbol{\nu}_{s|K}, \boldsymbol{\beta}_{s|K}, \theta_s) = \sum_{i=1}^n \ln f_{z\text{inb}}(x_{is}; \mu_{is}, \theta_s, \pi_{is} | \mathbf{x}_{K \setminus \{s\}}^{(i)}).$$

To solve this standard regression problem, we alternate the estimation of the dispersion parameter  $\theta_s$  and of parameters  $(\boldsymbol{\nu}_{s|K}, \boldsymbol{\beta}_{s|K})$ , as done in *Risso and others (2018)*. Specifically, after initialization, we iterate the following two steps until convergence (for the reader's convenience, we drop the index  $K$ ). Note that this procedure can be performed independently and in parallel for each regression performed within the structure learning strategy.



Step 1: **dispersion optimization.** Let  $\ln \theta_s = \zeta_s$ , we estimate parameter  $\zeta_s$  by solving the following problem

$$\hat{\zeta}_s \leftarrow \operatorname{argmax}_{\zeta_s} \{\ell_s(\hat{\boldsymbol{\beta}}_s, \hat{\boldsymbol{\nu}}_s, \theta_s)\}.$$

A first initial value for  $\zeta_s$ ,  $\zeta_s^0$  say, is found by applying the method of moments. If the moment estimator does not exist, as in the Poisson case,  $\zeta_s^0$  is assigned to the value that maximizes the objective function  $\ell_s(\hat{\boldsymbol{\nu}}_s, \hat{\boldsymbol{\beta}}_s, \zeta_s)$  over a suitable interval. In practice, we use **optimize** function in R over the range  $[-100, 100]$ . Once the initial value  $\zeta_s^0$  is fixed, we optimize  $\ell_s(\hat{\boldsymbol{\nu}}_s, \hat{\boldsymbol{\beta}}_s, \zeta_s)$  by a quasi-Newton optimization scheme.

The gradient of the objective function used by the optimization procedure is found as follows. The derivative of the negative binomial log density is:

$$\frac{\partial}{\partial \theta} \ln f_{nb}(y, \mu, \theta) = \Psi(y + \theta) - \Psi(\theta) + \ln \theta + 1 - \ln(\mu + \theta) - \frac{y + \theta}{\mu + \theta},$$

where  $\Psi(\theta) = \Gamma'(\theta)/\Gamma(\theta)$  is the digamma function. Hence, the derivative of the zinb model for  $\pi \in [0, 1]$  can be written as follows:

- for  $y > 0$ ,  $f_{zinb}(y, \mu, \theta, \pi) = (1 - \pi)f_{nb}(y, \mu, \theta)$ , so that

$$\frac{\partial}{\partial \theta} \ln f_{zinb}(y, \mu, \theta, \pi) = \Psi(y + \theta) - \Psi(\theta) + \ln \theta + 1 - \ln(\mu + \theta) - \frac{y + \theta}{\mu + \theta};$$

- for  $y = 0$ ,  $f_{zinb}(0, \mu, \theta, \pi) = \pi + (1 - \pi)f_{nb}(0, \mu, \theta)$ , so that

$$\begin{aligned} \frac{\partial}{\partial \theta} \ln f_{zinb}(0, \mu, \theta, \pi) &= \frac{(1 - \pi)f_{nb}(0, \mu, \theta) \frac{\partial}{\partial \theta} \ln f_{nb}(0, \mu, \theta)}{\pi + (1 - \pi)f_{nb}(0, \mu, \theta)} \\ &= \frac{\ln \theta + 1 - \ln(\mu + \theta) - \frac{\theta}{\mu + \theta}}{\frac{\pi(\mu + \theta)^\theta}{(1 - \pi)\theta^\theta} + 1}, \end{aligned}$$

Therefore, the derivative of the objective function w.r.t.  $\zeta_s$  for each response  $X_s$ ,  $s = 1, \dots, p$ , is

$$\sum_{i=1}^n \theta_s \frac{\partial}{\partial \theta} \ln f_{zinb}(x_{is}, \mu_{is}, \theta_s, \pi_{is}).$$

Step 2: **log-likelihood optimization.** Given a collection of  $n$  samples drawn from the random vector  $\mathbf{X}$ ,  $\mathbb{X}$  say, and dispersion parameter  $\hat{\zeta}_s \in \mathbb{R}$ , we estimate parameter  $(\boldsymbol{\beta}_s, \boldsymbol{\nu}_s)$  by solving the following problem

$$(\hat{\boldsymbol{\beta}}_s, \hat{\boldsymbol{\nu}}_s) \leftarrow \operatorname{argmax}_{(\boldsymbol{\beta}_s, \boldsymbol{\nu}_s)} \{\ell_s(\boldsymbol{\nu}_s, \boldsymbol{\beta}_s, \hat{\zeta}_s)\}. \quad (1.4)$$

For convenience, we reparameterize the log-likelihood as follows, as done in Risso *and others* (2018):

$$\begin{aligned} \ln(\mu_s) &= A_\mu a_\mu \\ \operatorname{logit}(1 - \pi_s) &= A_\pi a_\pi, \end{aligned}$$

where

$$\begin{cases} a_\mu &= (\nu_s^\mu, (\boldsymbol{\beta}_s^\mu)^T)^T \\ a_\pi &= (\nu_s^\pi, (\boldsymbol{\beta}_s^\pi)^T)^T \\ A_\mu &= (\mathbf{1}, \mathbb{X}_{\{K \setminus \{s\}\}}) \\ A_\pi &= (\mathbf{1}, \mathbb{X}_{\{K \setminus \{s\}\}}). \end{cases}$$

Therefore, Problem (1.4) translates into finding a set of vectors  $(a_\mu, a_\pi)$  that locally maximizes the log-likelihood of a zinb model for a vector of count  $X_s$ , i.e.,  $F(a_\mu, a_\pi) = \ell_s(\boldsymbol{\nu}_s, \boldsymbol{\beta}_s, \hat{\zeta}_s)$ .

Starting from an initial value, we perform a local maximization of this function  $F$  using BFGS method (Broyden, 1970; Fletcher, 1970; Goldfarb, 1970; Shanno, 1970). We first explicit the derivatives of the log-likelihood w.r.t. parameters  $(\mu, \pi)$  in the zinb distribution. We note that

$$f_{zinb}(y; \mu, \theta, \pi) = \pi \delta_0(y) + (1 - \pi) f_{nb}(y, \mu, \theta),$$

and

$$\frac{\partial}{\partial \mu} \ln f_{nb}(y, \mu, \theta) = \frac{y}{\theta} - \frac{y + \theta}{\theta + \mu},$$

so that

$$\begin{aligned} \frac{\partial}{\partial \mu} \ln f_{zinb}(y, \mu, \theta, \pi) &= \frac{(1 - \pi) f_{nb}(y, \mu, \theta) \frac{\partial}{\partial \mu} \ln f_{nb}(y, \mu, \theta)}{f_{zinb}(y, \mu, \theta, \pi)} \\ \frac{\partial}{\partial \pi} \ln f_{zinb}(y, \mu, \theta, \pi) &= \frac{\delta_0(y) - f_{nb}(y, \mu, \theta)}{f_{zinb}(y, \mu, \theta, \pi)}. \end{aligned}$$

Depending on whether  $y$  is equal to zero, the above given expressions become:

-  $y > 0$ : here,  $\delta_0(y) = 0$  and  $f_{zinb}(y, \mu, \theta, \pi) = (1 - \pi) f_{nb}(y, \mu, \theta)$ , so that one has

$$\begin{aligned} \frac{\partial}{\partial \mu} \ln f_{zinb}(y, \mu, \theta, \pi) &= \frac{y}{\theta} - \frac{y + \theta}{\theta + \mu} \\ \frac{\partial}{\partial \pi} \ln f_{zinb}(y, \mu, \theta, \pi) &= \frac{-1}{1 - \pi}. \end{aligned}$$

-  $y = 0$ : here,  $\delta_0(y) = 1$  and  $f_{zinb}(0, \mu, \theta, \pi) = \pi + (1 - \pi) f_{nb}(0, \mu, \theta)$ , and one has

$$\begin{aligned} \frac{\partial}{\partial \mu} \ln f_{zinb}(y, \mu, \theta, \pi) &= \frac{-(1 - \pi) \left( \frac{\theta}{\theta + \mu} \right)^{\theta + 1}}{\pi + (1 - \pi) \left( \frac{\theta}{\theta + \mu} \right)^\theta} \\ \frac{\partial}{\partial \pi} \ln f_{zinb}(y, \mu, \theta, \pi) &= \frac{1 - \left( \frac{\theta}{\theta + \mu} \right)^\theta}{\pi + (1 - \pi) \left( \frac{\theta}{\theta + \mu} \right)^\theta}. \end{aligned}$$

Using standard calculus for the differential of compositions and the fact that:

$$\begin{aligned} (\ln^{-1})'(\ln \mu) &= \mu \\ (\text{logit}^{-1})'(\text{logit}(1 - \pi)) &= -\pi(1 - \pi), \end{aligned}$$

one obtains

$$\begin{aligned} \nabla_{a_\mu} F &= A_\mu^T G \\ \nabla_{a_\pi} F &= A_\pi^T H, \end{aligned}$$

where  $G$  and  $H$  are the  $n$ -dimensional vectors given by

$$G_i = \mu_{is} \frac{\partial}{\partial \mu_{is}} \ln f_{z\text{inb}}(x_{is}, \mu_{is}, \theta_s, \pi_{is})$$

$$H_i = -\pi_{is}(1 - \pi_{is}) \frac{\partial}{\partial \pi_{is}} \ln f_{z\text{inb}}(x_{is}, \mu_{is}, \theta_s, \pi_{is}).$$

REMARK 1.1 Note that for each  $s \in V$ , the dispersion parameter  $\theta_s$  is constant, i.e.,  $\theta_s$  does not depend on conditional sets  $K$ . Hence, in practice, we estimate  $\theta_s$  by applying the above given procedure for  $K = V$ . Then, we use this estimate  $\hat{\theta}_s$  as the input of the second step, log-likelihood optimization.

REMARK 1.2 It is worth to note that: (i) for negative binomial models, i.e.,  $\pi_{s|K} = 0, \forall s \in K \subseteq V$ , parameters are estimated similarly by considering  $a_\pi$  as a vector 0, and  $A_\pi$  as a matrix  $\mathbf{0}$ ; (ii) negative binomial distributions belong to the exponential family. Hence, an alternative way to estimate parameters is the iteratively reweighted least squares (IRWLS) algorithm. This approach does not depend on the choice of initial values for parameters. As a result, PC-nb using IRWLS algorithm, called PC-nbgml could be more accurate in some scenarios with significantly reduced computational time (see Table S7). In practice, when dealing with high dimensional data, we suggest users to use the PC-nbgml algorithm.

### 1.3 Identifiability of zero-inflated negative binomial distributions

In this section, we prove that the zinb model is identifiable.

THEOREM 1.3 Assume  $X$  follows a zinb distribution, i.e.,  $X \sim \text{zinb}(\pi, \theta, \mu)$ . Then, the density function of  $X$  is identifiable.

*Proof.* We prove the theorem by contradiction. Assume there exists  $(\pi_1, \theta_1, \mu_1) \neq (\pi_2, \theta_2, \mu_2)$  such that  $X_1 \sim \text{zinb}(\pi_1, \theta_1, \mu_1)$  with density function  $f_1(\cdot, \pi_1, \theta_1, \mu_1)$ ;  $X_2 \sim \text{zinb}(\pi_2, \theta_2, \mu_2)$  with density function  $f_2(\cdot, \pi_2, \theta_2, \mu_2)$ , and  $f_1(\cdot, \pi_1, \theta_1, \mu_1) \equiv f_2(\cdot, \pi_2, \theta_2, \mu_2)$ .

For  $s = 1, 2$ , one has  $f_s(x_s, \mu_s, \theta_s, \pi_s) = \pi_s \delta_0(x_s) + (1 - \pi_s) f_{nb}(x_s, \mu_s, \theta_s)$ . Let  $x_s = 0, 1, 2, 3$ , then

$$\pi_1 + (1 - \pi_1) \left( \frac{\theta_1}{\theta_1 + \mu_1} \right)^{\theta_1} = \pi_2 + (1 - \pi_2) \left( \frac{\theta_2}{\theta_2 + \mu_2} \right)^{\theta_2} \quad (1.5)$$

$$(1 - \pi_1) \frac{\Gamma(1 + \theta_1)}{\Gamma(2)\Gamma(\theta_1)} \left( \frac{\theta_1}{\theta_1 + \mu_1} \right)^{\theta_1} \left( \frac{\mu_1}{\theta_1 + \mu_1} \right) = (1 - \pi_2) \frac{\Gamma(1 + \theta_2)}{\Gamma(2)\Gamma(\theta_2)} \left( \frac{\theta_2}{\theta_2 + \mu_2} \right)^{\theta_2} \left( \frac{\mu_2}{\theta_2 + \mu_2} \right)$$

$$(1 - \pi_1) \frac{\Gamma(2 + \theta_1)}{\Gamma(3)\Gamma(\theta_1)} \left( \frac{\theta_1}{\theta_1 + \mu_1} \right)^{\theta_1} \left( \frac{\mu_1}{\theta_1 + \mu_1} \right)^2 = (1 - \pi_2) \frac{\Gamma(2 + \theta_2)}{\Gamma(3)\Gamma(\theta_2)} \left( \frac{\theta_2}{\theta_2 + \mu_2} \right)^{\theta_2} \left( \frac{\mu_2}{\theta_2 + \mu_2} \right)^2$$

$$(1 - \pi_1) \frac{\Gamma(3 + \theta_1)}{\Gamma(4)\Gamma(\theta_1)} \left( \frac{\theta_1}{\theta_1 + \mu_1} \right)^{\theta_1} \left( \frac{\mu_1}{\theta_1 + \mu_1} \right)^3 = (1 - \pi_2) \frac{\Gamma(3 + \theta_2)}{\Gamma(4)\Gamma(\theta_2)} \left( \frac{\theta_2}{\theta_2 + \mu_2} \right)^{\theta_2} \left( \frac{\mu_2}{\theta_2 + \mu_2} \right)^3.$$

One has

$$\frac{f_1(2, \pi_1, \theta_1, \mu_1)}{f_1(1, \pi_1, \theta_1, \mu_1)} = \frac{f_2(2, \pi_2, \theta_2, \mu_2)}{f_2(1, \pi_2, \theta_2, \mu_2)}$$

$$\Rightarrow \frac{\Gamma(2 + \theta_1)}{\Gamma(1 + \theta_1)} \left( \frac{\mu_1}{\theta_1 + \mu_1} \right) = \frac{\Gamma(2 + \theta_2)}{\Gamma(1 + \theta_2)} \left( \frac{\mu_2}{\theta_2 + \mu_2} \right). \quad (1.6)$$

As  $\Gamma(z + 1) = z\Gamma(z)$ , Equation 1.6 yields

$$(1 + \theta_1) \left( \frac{\mu_1}{\theta_1 + \mu_1} \right) = (1 + \theta_2) \left( \frac{\mu_2}{\theta_2 + \mu_2} \right). \quad (1.7)$$

Similarly,

$$\begin{aligned} \frac{f_1(3, \pi_1, \theta_1, \mu_1)}{f_1(2, \pi_1, \theta_1, \mu_1)} &= \frac{f_2(3, \pi_2, \theta_2, \mu_2)}{f_2(2, \pi_2, \theta_2, \mu_2)} \\ \Rightarrow (2 + \theta_1) \left( \frac{\mu_1}{\theta_1 + \mu_1} \right) &= (2 + \theta_2) \left( \frac{\mu_2}{\theta_2 + \mu_2} \right). \end{aligned} \quad (1.8)$$

From Equation (1.7) and Equation (1.8), one gets

$$\frac{\mu_1}{\theta_1 + \mu_1} = \frac{\mu_2}{\theta_2 + \mu_2}. \quad (1.9)$$

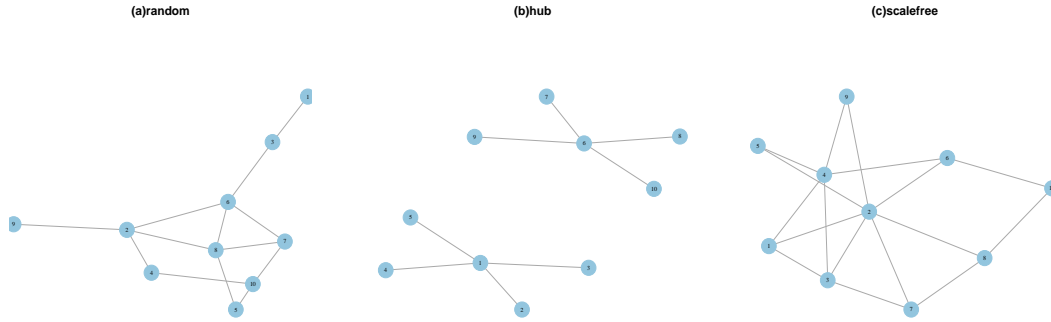
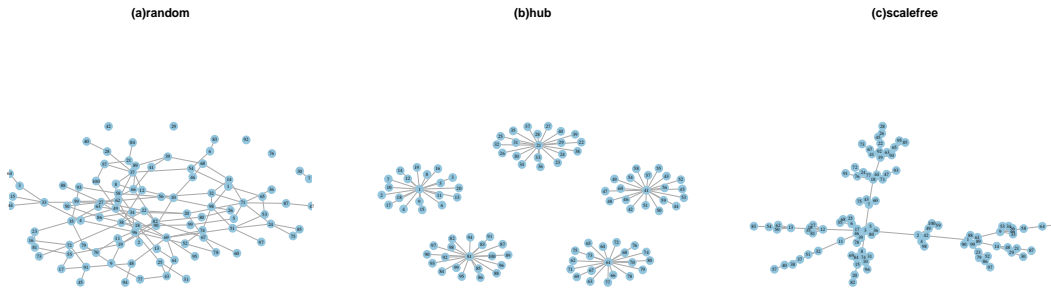
Finally, Equation (1.5), (1.7), and (1.9) yield  $(\pi_1, \theta_1, \mu_1) = (\pi_2, \theta_2, \mu_2)$ , that contradicts the Assumption.  $\square$

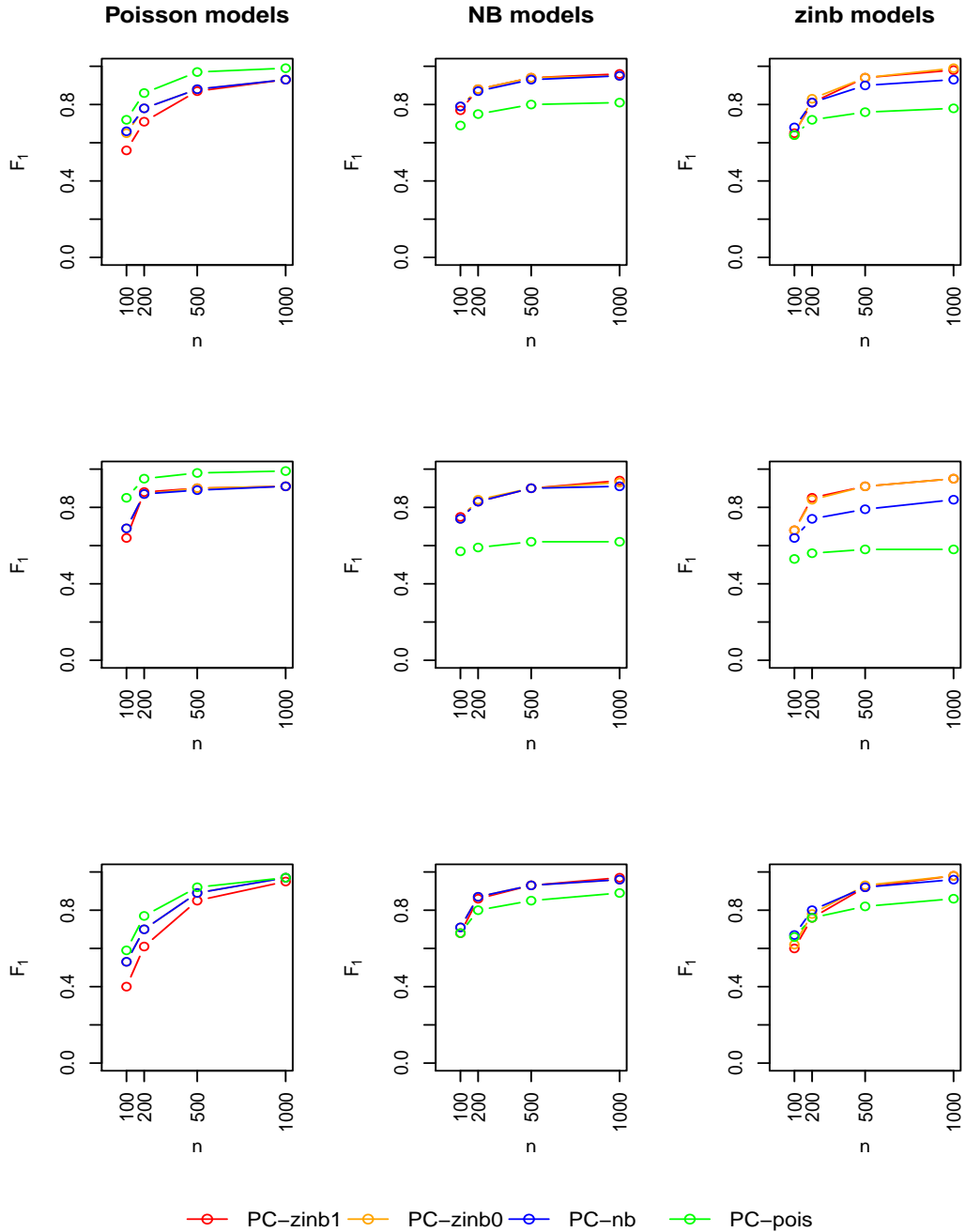
## 2. REAL DATA ANALYSIS

Our analysis focusses on the total set of 1543 transcription factors (TF), which are known to play a central role in the regulation of other genes (Fletcher *and others*, 2017). As measurements were zero-inflated and highly skewed, with total count volumes depending on experimental condition, standard preprocessing was applied to the data as in Allen and Liu (2013); Nguyen and Chiogna (2018). In particular, we filtered out the genes with the mean smaller than 0.005; normalized the data by 95% quantile matching; selected the top 1000 cells with the highest mean from the groups that had more than 1000 cells; and used a power transform  $X^\alpha$  (with  $\alpha = 0.5$ ).

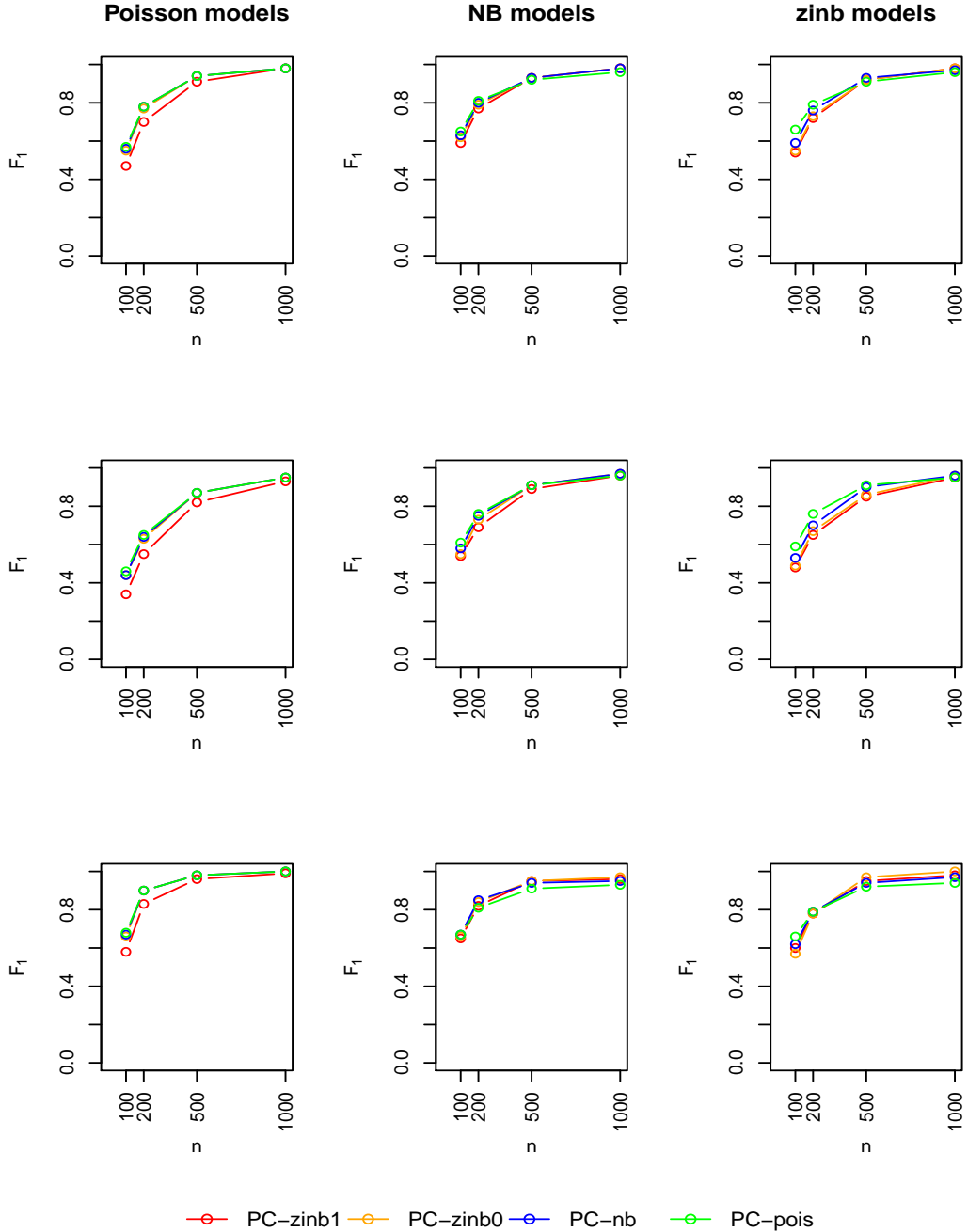
Normalized data were used as input to PC-zinb1 with a significance level of  $\alpha = 2(1 - \Phi(n^{0.15}))$  (Nguyen and Chiogna, 2018), and the maximum cardinality of conditional independence set  $m = 3$ . Once estimated, we extracted the 2-core of the networks by iteratively excluding transcription factors with fewer than 2 edges, leaving a network with 926, 991, 465 and 772 genes for the HBC\*, GBC, iOSN and mOSN cell types, respectively. For each network, we performed community detection using the Leiden algorithm (Traag *and others*, 2019), where we supervise the resolution parameter to be 0.4 for HBC\*, GBC and mOSN, and 0.25 for the iOSN network, as a resolution parameter of 0.4 resulted in a too high number of communities there. The transcription factors in each of these communities were then used in an overrepresentation analysis using the biological processes hallmark gene sets of the MSigDB database (Subramanian *and others*, 2005; Liberzon *and others*, 2015), where only gene sets containing at least 5 genes were retained. We ranked gene sets using a Fisher's exact test, and only the top 10 enriched gene sets were interpreted.

## 3. SUPPLEMENTARY FIGURES AND TABLES

Supplementary Fig. S1. The graph structures for  $p = 10$  employed in the simulation studies.Supplementary Fig. S2. The graph structures for  $p = 100$  employed in the simulation studies.



Supplementary Fig. S3.  $F_1$ -score of the considered algorithms for the three types of graphs in Supplementary Figure S1 with  $p = 10, \mu = 5, \theta = 0.5$ : random (top); hub (middle); scale-free (bottom). PC-zinb1: zinb model in which the structure of the graph is attributable to both of the two parameter components  $\mu_{s|K}$  and  $\pi_{s|K}$ ; PC-zinb0: zinb model in which the structure of the graph is attributable to only the parameter component  $\mu_{s|K}$  and consider  $\pi_{s|K}$  as a constant; PC-nb: Negative binomial model, i.e., the special case of zinb models where  $\pi_{s|K} = 0$ ; PC-pois: Poisson model of Nguyen and Chiogna (2018).



Supplementary Fig. S4.  $F_1$ -score of the considered algorithms for the three types of graphs in Supplementary Figure S1 with  $p = 10$ ,  $\mu = 0.5$ ,  $\theta = 0.5$ : random (top); hub (middle); scale-free (bottom). PC-zinb1: zinb model in which the structure of the graph is attributable to both of the two parameter components  $\mu_{s|K}$  and  $\pi_{s|K}$ ; PC-zinb0: zinb model in which the structure of the graph is attributable to only the parameter component  $\mu_{s|K}$  and consider  $\pi_{s|K}$  as a constant; PC-nb: Negative binomial model, i.e., the special case of zinb models where  $\pi_{s|K} = 0$ ; PC-pois: Poisson model of Nguyen and Chiogna (2018).

Supplementary Table S1. Monte Carlo means of Precision (P), Recall (R),  $F_1$ -score, and runtime obtained by simulating 50 samples from three different types of graphs in Figure S2 ( $p = 100$ ), under zinb node conditional distribution mean  $\mu = 0.5, 5; \theta = 0.5$  and levels of noise  $\mu_{noise} = 0.5$ . The levels of significance of tests  $\alpha = 2(1 - \Phi(\eta^{0.2}))$  for  $n = 500, 1000$ , and  $\alpha = 2(1 - \Phi(\eta^{0.225}))$  for  $n = 200$ .

$\mu$	type	$n$	PC-zinb1				PC-zinb0				PC-nb				PC-Poisson			
			P	R	$F_1$	time	P	R	$F_1$	time	P	R	$F_1$	time	P	R	$F_1$	time
0.5	scalefree	200	0.86	0.30	0.44	16.18	0.72	0.32	0.44	12.79	0.46	0.50	0.48	5.41	0.51	0.55	0.53	2.80
		500	0.85	0.72	0.78	30.50	0.85	0.71	0.77	24.21	0.77	0.81	0.79	16.75	0.63	0.85	0.72	5.21
		1000	0.96	0.88	0.92	72.20	0.96	0.87	0.91	60.85	0.95	0.91	0.93	53.93	0.80	0.95	0.87	9.36
	hub	200	0.76	0.13	0.21	17.15	0.46	0.15	0.23	13.66	0.22	0.23	0.22	6.16	0.25	0.25	0.25	3.33
		500	0.68	0.38	0.49	69.81	0.70	0.42	0.52	52.35	0.64	0.55	0.59	40.36	0.46	0.60	0.52	16.50
		1000	0.92	0.68	0.78	460.61	0.92	0.70	0.80	321.04	0.90	0.82	0.86	216.20	0.72	0.86	0.79	71.09
	random	200	0.83	0.24	0.38	15.62	0.72	0.27	0.40	12.62	0.54	0.47	0.50	5.60	0.59	0.52	0.55	2.84
		500	0.89	0.67	0.76	28.31	0.90	0.67	0.76	23.02	0.85	0.77	0.81	14.79	0.74	0.85	0.79	4.49
		1000	0.97	0.88	0.93	55.79	0.98	0.88	0.93	46.93	0.96	0.94	0.95	31.41	0.88	0.97	0.92	6.39
5	scalefree	200	0.45	0.56	0.50	63.61	0.17	0.69	0.28	417.34	0.28	0.71	0.40	109.36	0.15	0.86	0.25	196.19
		500	0.85	0.87	0.86	57.41	0.80	0.88	0.84	60.98	0.44	0.92	0.59	54.89	0.13	0.98	0.23	461.16
		1000	0.96	0.95	0.95	154.38	0.94	0.96	0.95	133.03	0.55	0.97	0.70	118.11	0.14	1.00	0.25	473.77
	hub	200	0.26	0.32	0.28	115.31	0.09	0.40	0.15	568.91	0.15	0.42	0.22	195.42	0.09	0.63	0.16	344.34
		500	0.73	0.77	0.75	2798.25	0.67	0.80	0.73	2119.00	0.30	0.85	0.45	1115.44	0.10	0.95	0.18	2103.79
		1000	0.90	0.97	0.93	2701.99	0.86	0.98	0.91	1917.64	0.43	0.99	0.60	1614.48	0.11	1.00	0.20	1132.43
	random	200	0.54	0.49	0.49	121.16	0.22	0.67	0.33	566.84	0.40	0.63	0.49	85.50	0.19	0.84	0.31	219.67
		500	0.91	0.85	0.88	40.05	0.77	0.84	0.81	97.37	0.60	0.93	0.73	39.03	0.18	0.99	0.31	470.34
		1000	0.98	0.97	0.97	84.68	0.97	0.97	0.97	70.19	0.73	0.99	0.84	59.62	0.20	1.00	0.34	442.33



Supplementary Table S2. Monte Carlo means of Precision (P), Recall (R),  $F_1$ -score, and runtime obtained by simulating 50 samples from three different types of graphs in Figure S2 ( $p = 100$ ), under NB node conditional distribution mean  $\mu = 0.5, 5; \theta = 0.5$  and levels of noise  $\mu_{noise} = 0.5$ . The levels of significance of tests  $\alpha = 2(1 - \Phi(n^{0.2}))$  for  $n = 500, 1000$ , and  $\alpha = 2(1 - \Phi(n^{0.225}))$  for  $n = 200$ .

$\mu$	type	$n$	PC-zinb1				PC-zinb0				PC-nb				PC-Poisson			
			P	R	$F_1$	time	P	R	$F_1$	time	P	R	$F_1$	time	P	R	$F_1$	time
0.5	scalefree	200	0.64	0.44	0.52	17.17	0.62	0.48	0.54	14.97	0.50	0.55	0.53	5.83	0.52	0.57	0.54	2.71
		500	0.81	0.80	0.80	41.22	0.78	0.82	0.80	35.76	0.68	0.85	0.76	13.53	0.66	0.86	0.75	4.57
		1000	0.94	0.92	0.93	101.87	0.94	0.93	0.94	89.41	0.89	0.94	0.92	40.50	0.85	0.95	0.90	8.85
	hub	200	0.31	0.13	0.19	16.05	0.34	0.20	0.25	15.57	0.23	0.22	0.23	6.17	0.24	0.23	0.24	2.83
		500	0.63	0.43	0.51	84.10	0.64	0.52	0.57	108.24	0.53	0.55	0.54	44.52	0.50	0.58	0.53	13.83
		1000	0.90	0.75	0.82	666.14	0.94	0.81	0.87	654.73	0.89	0.82	0.85	214.25	0.80	0.85	0.82	57.70
	random	200	0.68	0.38	0.48	17.49	0.65	0.41	0.50	15.26	0.59	0.49	0.53	6.00	0.60	0.52	0.55	2.69
		500	0.87	0.77	0.82	35.41	0.86	0.81	0.84	31.12	0.80	0.86	0.83	11.85	0.78	0.86	0.82	4.03
		1000	0.97	0.93	0.95	66.69	0.96	0.95	0.95	55.20	0.93	0.97	0.95	23.46	0.90	0.97	0.94	5.94
5	scalefree	200	0.58	0.85	0.69	147.76	0.52	0.86	0.65	260.75	0.51	0.86	0.64	106.25	0.16	0.89	0.28	118.22
		500	0.65	0.97	0.78	488.63	0.59	0.97	0.73	815.13	0.56	0.97	0.71	477.96	0.15	0.98	0.26	235.45
		1000	0.76	0.99	0.86	772.97	0.71	1.00	0.83	971.08	0.69	1.00	0.81	447.78	0.17	1.00	0.29	198.03
	hub	200	0.47	0.69	0.56	787.84	0.42	0.71	0.53	1199.39	0.40	0.70	0.51	403.94	0.11	0.67	0.18	219.03
		500	0.57	0.96	0.71	3255.89	0.51	0.97	0.67	4510.77	0.49	0.97	0.65	1605.72	0.12	0.96	0.21	568.49
		1000	0.69	1.00	0.82	5286.75	0.63	1.00	0.78	5839.82	0.63	1.00	0.77	2369.42	0.14	1.00	0.24	550.99
	random	200	0.61	0.77	0.68	55.95	0.52	0.80	0.63	105.08	0.54	0.80	0.64	40.06	0.22	0.88	0.35	127.11
		500	0.69	0.98	0.81	153.75	0.62	0.98	0.76	244.76	0.61	0.98	0.75	110.86	0.21	0.99	0.35	240.44
		1000	0.81	1.00	0.90	183.54	0.76	1.00	0.86	276.04	0.74	1.00	0.85	178.44	0.24	1.00	0.39	209.13

Supplementary Table S3. Monte Carlo means of Precision (P), Recall (R),  $F_1$ -score, and runtime obtained by simulating 50 samples from three different types of graphs in Figure S2 ( $p = 100$ ), under Poisson node conditional distribution with mean  $\lambda = 0.5, 5$ ; and levels of noise  $\lambda_{noise} = 0.5$ . The levels of significance of tests  $\alpha = 2(1 - \Phi(n^{0.2}))$  for  $n = 500, 1000$ , and  $\alpha = 2(1 - \Phi(n^{0.225}))$ .

$\lambda$	type	$n$	PC-zinb1				PC-zinb0				PC-nb				PC-Poisson			
			P	R	$F_1$	time	P	R	$F_1$	time	P	R	$F_1$	time	P	R	$F_1$	time
0.5	scalefree	200	0.89	0.20	0.32	19.24	0.93	0.29	0.44	18.02	0.91	0.30	0.45	4.74	0.92	0.33	0.48	2.38
		500	0.97	0.63	0.76	36.87	0.98	0.69	0.80	34.54	0.97	0.69	0.81	8.17	0.98	0.72	0.83	3.41
		1000	1.00	0.81	0.89	70.16	1.00	0.84	0.91	67.85	1.00	0.84	0.91	13.67	1.00	0.87	0.93	5.60
	hub	200	0.64	0.03	0.05	17.89	0.74	0.05	0.09	17.00	0.69	0.05	0.1	4.62	0.72	0.06	0.11	2.28
		500	0.89	0.13	0.22	32.59	0.93	0.20	0.33	31.94	0.92	0.21	0.34	8.20	0.93	0.22	0.36	3.39
		1000	0.99	0.30	0.46	72.05	0.99	0.45	0.62	104.98	0.99	0.46	0.63	21.97	0.99	0.47	0.64	10.43
	random	200	0.88	0.15	0.26	19.50	0.93	0.22	0.35	17.91	0.92	0.23	0.37	4.74	0.93	0.25	0.39	2.36
		500	0.98	0.57	0.72	35.74	0.98	0.65	0.78	33.03	0.98	0.66	0.79	7.92	0.98	0.67	0.80	3.19
		1000	1.00	0.83	0.90	63.65	1.00	0.87	0.93	58.93	1.00	0.88	0.93	12.80	1.00	0.88	0.94	4.95
5	scalefree	200	0.99	0.45	0.61	10.21	0.96	0.55	0.70	9.68	0.96	0.55	0.70	4.08	0.96	0.55	0.70	2.33
		500	1.00	0.79	0.88	19.92	0.99	0.84	0.91	20.26	0.99	0.84	0.91	7.06	0.99	0.84	0.91	3.42
		1000	1.00	0.90	0.94	39.09	0.99	0.92	0.95	41.58	0.99	0.92	0.95	11.28	0.99	0.92	0.95	5.89
	hub	200	0.84	0.05	0.09	8.93	0.76	0.11	0.19	8.91	0.74	0.11	0.19	3.92	0.75	0.11	0.19	2.22
		500	0.99	0.29	0.45	92.09	0.96	0.44	0.60	207.72	0.96	0.44	0.60	42.75	0.96	0.44	0.60	27.95
		1000	1.00	0.67	0.80	232.08	1.00	0.80	0.88	387.07	1.00	0.80	0.89	71.08	1.00	0.80	0.88	39.57
	random	200	0.98	0.30	0.46	10.02	0.96	0.43	0.60	9.67	0.96	0.44	0.60	3.92	0.96	0.43	0.60	2.29
		500	1.00	0.75	0.86	18.04	0.99	0.83	0.90	17.76	0.99	0.83	0.90	6.34	0.99	0.83	0.90	3.06
		1000	1.00	0.92	0.96	32.95	1.00	0.95	0.97	32.35	1.00	0.95	0.97	9.28	1.00	0.95	0.97	4.75

Supplementary Table S4. Monte Carlo means of Precision (P), Recall (R),  $F_1$ -score, and runtime obtained by simulating 50 samples from three different types of graphs in Figure S1 ( $p = 10$ ), under zinb node conditional models with mean  $\mu = 0.5, 5; \theta = 0.5$ , and levels of noise  $\mu^{noise} = 0.5$ . The levels of significance of tests  $\alpha = 2(1 - \Phi(n^{0.15}))$ .

$\mu$	type	$n$	PC-zinbI				PC-zinb0				PC-nb				PC-Poisson			
			P	R	$F_1$	time	P	R	$F_1$	time	P	R	$F_1$	time	P	R	$F_1$	time
0.5	scalefree	100	0.77	0.36	0.48	1.73	0.77	0.37	0.49	1.53	0.78	0.41	0.53	1.34	0.75	0.49	0.59	0.87
		200	0.91	0.51	0.65	2.06	0.92	0.54	0.67	1.82	0.89	0.58	0.70	1.67	0.87	0.68	0.76	0.99
		500	0.97	0.76	0.85	6.39	0.98	0.77	0.86	4.53	0.96	0.85	0.90	4.00	0.95	0.88	0.91	0.92
		1000	0.99	0.92	0.95	23.70	0.99	0.94	0.96	18.28	0.98	0.95	0.96	15.05	0.96	0.95	0.95	2.09
		100	0.68	0.56	0.60	1.69	0.66	0.52	0.57	1.52	0.65	0.62	0.62	1.34	0.65	0.70	0.66	0.87
		200	0.80	0.78	0.78	2.02	0.81	0.75	0.78	1.78	0.77	0.83	0.79	1.54	0.74	0.87	0.79	0.90
	hub	500	0.92	0.99	0.95	3.57	0.96	0.98	0.97	2.67	0.91	0.99	0.94	2.01	0.86	1.00	0.92	0.47
		1000	0.96	1.00	0.98	5.13	0.99	1.00	1.00	3.53	0.94	1.00	0.97	2.72	0.90	1.00	0.94	0.94
		100	0.74	0.43	0.54	1.63	0.74	0.45	0.55	1.51	0.74	0.49	0.59	1.31	0.74	0.60	0.66	0.85
		200	0.85	0.63	0.72	2.00	0.87	0.63	0.73	1.68	0.85	0.69	0.76	1.47	0.82	0.77	0.79	0.89
		500	0.95	0.89	0.92	3.33	0.98	0.88	0.92	2.53	0.95	0.91	0.93	2.16	0.89	0.92	0.91	0.48
		1000	0.99	0.97	0.98	4.94	0.99	0.97	0.98	3.67	0.96	0.98	0.97	2.91	0.93	0.98	0.96	1.00
5	scalefree	100	0.78	0.49	0.60	1.90	0.81	0.51	0.62	1.74	0.73	0.62	0.67	1.69	0.59	0.76	0.66	1.32
		200	0.89	0.67	0.76	2.93	0.89	0.70	0.78	2.95	0.83	0.78	0.80	2.50	0.66	0.89	0.76	1.61
		500	0.95	0.89	0.92	9.68	0.96	0.91	0.93	7.83	0.90	0.94	0.92	7.90	0.71	0.97	0.82	1.92
		1000	0.98	0.98	0.98	36.61	0.97	0.99	0.98	29.87	0.94	1.00	0.96	19.64	0.76	0.99	0.86	3.24
		100	0.63	0.77	0.68	1.97	0.64	0.74	0.68	1.70	0.50	0.88	0.64	1.62	0.37	0.94	0.53	1.23
		200	0.79	0.94	0.85	2.47	0.77	0.94	0.84	2.19	0.60	0.98	0.74	2.08	0.40	0.99	0.56	1.34
	hub	500	0.84	1.00	0.91	3.38	0.84	1.00	0.91	2.84	0.66	1.00	0.79	2.52	0.41	1.00	0.58	1.02
		1000	0.91	1.00	0.95	5.21	0.91	1.00	0.95	4.15	0.72	1.00	0.84	3.45	0.41	1.00	0.58	1.73
		100	0.74	0.59	0.65	1.78	0.73	0.58	0.64	1.62	0.68	0.69	0.68	1.53	0.52	0.82	0.64	1.25
		200	0.87	0.77	0.81	2.21	0.88	0.79	0.83	1.95	0.77	0.85	0.81	1.85	0.58	0.93	0.72	1.36
		500	0.94	0.95	0.94	3.86	0.94	0.95	0.94	3.16	0.85	0.96	0.90	2.77	0.62	0.98	0.76	1.16
		1000	0.97	1.00	0.98	6.00	0.97	1.00	0.99	4.83	0.88	0.99	0.93	4.21	0.64	1.00	0.78	1.78
random	100	0.74	0.59	0.65	1.78	0.73	0.58	0.64	1.62	0.68	0.69	0.68	1.53	0.52	0.82	0.64	1.25	
	200	0.87	0.77	0.81	2.21	0.88	0.79	0.83	1.95	0.77	0.85	0.81	1.85	0.58	0.93	0.72	1.36	
	500	0.94	0.95	0.94	3.86	0.94	0.95	0.94	3.16	0.85	0.96	0.90	2.77	0.62	0.98	0.76	1.16	
	1000	0.97	1.00	0.98	6.00	0.97	1.00	0.99	4.83	0.88	0.99	0.93	4.21	0.64	1.00	0.78	1.78	

Supplementary Table S5. Monte Carlo means of Precision (P), Recall (R),  $F_1$ -score, and runtime obtained by simulating 50 samples from three different types of graphs in Figure S1 ( $p = 10$ ), under NB node conditional models with mean  $\mu = 0.5, 5; \theta = 0.5$ , and levels of noise  $\mu_{noise} = 0.5$ . The levels of significance of tests  $\alpha = 2(1 - \Phi(n^{0.15}))$ .

$\mu$	type	$n$	PC-zinb1			PC-zinb0			PC-nb			PC-Poisson						
			P	R	$F_1$	time	P	R	$F_1$	time	P	R	$F_1$	time				
0.5	scalefree	100	0.77	0.42	0.54	1.88	0.80	0.42	0.55	1.77	0.79	0.46	0.58	1.38	0.77	0.51	0.61	0.87
		500	0.90	0.56	0.69	2.41	0.92	0.60	0.73	2.23	0.91	0.64	0.75	1.67	0.88	0.67	0.76	0.95
		500	0.96	0.83	0.89	7.22	0.96	0.86	0.91	6.84	0.96	0.87	0.91	3.70	0.94	0.88	0.91	0.94
		1000	0.98	0.94	0.96	18.66	0.99	0.95	0.97	16.74	0.98	0.96	0.97	11.02	0.97	0.96	0.96	2.25
		100	0.68	0.65	0.65	1.92	0.69	0.66	0.66	1.74	0.68	0.68	0.67	1.36	0.62	0.76	0.67	0.88
		200	0.81	0.84	0.82	2.32	0.83	0.87	0.84	2.04	0.80	0.90	0.85	1.56	0.72	0.92	0.81	0.90
	random	500	0.91	1.00	0.95	3.52	0.92	0.99	0.95	2.87	0.90	1.00	0.94	2.00	0.85	1.00	0.91	0.49
		1000	0.93	1.00	0.96	4.88	0.94	1.00	0.97	3.91	0.91	1.00	0.95	2.57	0.87	1.00	0.93	0.95
		100	0.76	0.49	0.59	1.77	0.78	0.52	0.62	1.60	0.77	0.54	0.63	1.32	0.73	0.60	0.65	0.84
		200	0.87	0.70	0.77	2.22	0.89	0.71	0.79	1.83	0.89	0.74	0.80	1.42	0.85	0.78	0.81	0.87
		500	0.96	0.91	0.93	3.06	0.95	0.92	0.93	2.67	0.94	0.93	0.93	1.92	0.91	0.94	0.92	0.47
		1000	0.98	0.98	0.98	4.54	0.97	0.99	0.98	3.72	0.96	0.99	0.98	2.33	0.94	0.99	0.96	0.95
5	scalefree	100	0.74	0.63	0.68	3.10	0.73	0.69	0.71	4.03	0.73	0.70	0.71	2.18	0.61	0.76	0.68	1.35
		500	0.87	0.86	0.86	6.02	0.85	0.89	0.87	7.83	0.85	0.89	0.87	3.98	0.72	0.92	0.80	1.54
		500	0.91	0.96	0.93	17.39	0.90	0.97	0.93	19.74	0.90	0.97	0.93	9.82	0.75	0.98	0.85	1.97
		1000	0.95	0.99	0.97	39.63	0.94	0.99	0.96	46.62	0.94	0.99	0.96	36.91	0.81	1.00	0.89	3.23
		100	0.64	0.91	0.75	2.49	0.62	0.93	0.74	2.64	0.62	0.94	0.74	1.69	0.40	0.97	0.57	1.20
		200	0.72	1.00	0.83	3.03	0.73	1.00	0.84	2.97	0.72	1.00	0.83	1.84	0.42	1.00	0.59	1.19
	random	500	0.83	1.00	0.90	4.13	0.83	1.00	0.90	3.77	0.82	1.00	0.90	2.29	0.45	1.00	0.62	0.82
		1000	0.89	1.00	0.94	6.55	0.87	1.00	0.93	5.95	0.85	1.00	0.91	3.45	0.45	1.00	0.62	1.36
		100	0.76	0.79	0.77	2.44	0.76	0.83	0.79	2.44	0.76	0.83	0.79	1.57	0.58	0.88	0.69	1.14
		200	0.85	0.91	0.88	3.14	0.83	0.93	0.88	2.94	0.83	0.93	0.87	1.87	0.62	0.95	0.75	1.24
		500	0.90	0.99	0.94	4.94	0.89	1.00	0.94	4.58	0.88	0.99	0.93	2.71	0.67	1.00	0.80	0.92
		1000	0.92	1.00	0.96	7.91	0.92	1.00	0.95	6.54	0.92	1.00	0.95	3.98	0.69	1.00	0.81	1.51

Supplementary Table S6. Monte Carlo means of Precision (P), Recall (R),  $F_1$ -score, and runtime obtained by simulating 50 samples from three different types of graphs in Figure S1 ( $p = 10$ ), under Poisson node conditional model with mean  $\lambda = 0.5, 5$ ; and levels of noise  $\lambda_{noise} = 0.5$ . The levels of significance of tests  $\alpha = 2(1 - \Phi(n^{0.15}))$ .

$\lambda$	type	$n$	PC-zinb1			PC-zinb0			PC-nb			PC-Poisson						
			P	R	$F_1$	time	P	R	$F_1$	time	P	R	$F_1$	time				
0.5	scalefree	100	0.82	0.22	0.34	1.63	0.86	0.30	0.44	1.58	0.85	0.31	0.44	1.27	0.86	0.32	0.46	0.80
		500	0.93	0.40	0.55	1.85	0.95	0.48	0.63	1.79	0.95	0.49	0.64	1.34	0.96	0.50	0.65	0.83
		500	0.98	0.71	0.82	4.20	0.99	0.77	0.87	4.02	0.99	0.78	0.87	1.91	0.99	0.79	0.87	0.61
		1000	1.00	0.88	0.93	11.75	1.00	0.91	0.95	11.75	1.00	0.91	0.95	3.46	1.00	0.92	0.95	1.62
		100	0.73	0.50	0.58	1.75	0.81	0.57	0.66	1.64	0.81	0.58	0.67	1.28	0.81	0.60	0.68	0.82
		200	0.89	0.78	0.83	2.29	0.95	0.86	0.90	2.00	0.95	0.86	0.90	1.34	0.94	0.86	0.90	0.86
	hub	500	0.94	0.99	0.96	3.20	0.97	1.00	0.98	2.74	0.97	1.00	0.98	1.48	0.97	1.00	0.98	0.42
		1000	0.99	1.00	0.99	4.21	0.99	1.00	1.00	3.71	0.99	1.00	1.00	1.65	0.99	1.00	1.00	0.90
		100	0.77	0.35	0.47	1.68	0.85	0.42	0.55	1.59	0.84	0.43	0.56	1.26	0.84	0.44	0.57	0.80
		200	0.90	0.59	0.70	1.80	0.94	0.66	0.77	1.71	0.94	0.67	0.78	1.30	0.95	0.68	0.78	0.82
		500	0.98	0.85	0.91	2.90	0.98	0.90	0.94	2.69	0.98	0.90	0.94	1.46	0.99	0.90	0.94	0.41
		1000	1.00	0.96	0.98	4.25	1.00	0.97	0.98	3.65	1.00	0.97	0.98	1.70	1.00	0.97	0.98	0.91
5	scalefree	100	0.97	0.26	0.40	1.48	0.90	0.38	0.53	1.55	0.90	0.38	0.53	1.32	0.91	0.45	0.59	0.82
		200	0.99	0.46	0.61	1.70	0.97	0.57	0.70	1.91	0.97	0.57	0.70	1.43	0.97	0.64	0.77	0.87
		500	1.00	0.75	0.85	3.42	0.99	0.82	0.89	3.90	0.99	0.82	0.89	1.95	0.99	0.86	0.92	0.68
		1000	1.00	0.90	0.95	9.76	1.00	0.94	0.97	12.64	1.00	0.95	0.97	3.48	1.00	0.95	0.97	1.86
		100	0.94	0.52	0.64	1.53	0.85	0.63	0.69	1.58	0.85	0.63	0.69	1.32	0.87	0.84	0.85	0.84
		200	0.98	0.83	0.88	1.84	0.93	0.86	0.87	1.80	0.93	0.86	0.87	1.40	0.93	0.98	0.95	0.87
	hub	500	0.99	0.87	0.90	2.30	0.97	0.87	0.90	2.22	0.97	0.87	0.89	1.53	0.97	1.00	0.98	0.42
		1000	1.00	0.88	0.91	2.89	0.99	0.88	0.91	2.78	0.99	0.88	0.91	1.71	0.99	1.00	0.99	0.90
		100	0.95	0.41	0.56	1.50	0.91	0.53	0.65	1.52	0.91	0.54	0.66	1.31	0.91	0.60	0.72	0.80
		200	0.99	0.58	0.71	1.61	0.95	0.68	0.78	1.67	0.95	0.69	0.78	1.37	0.95	0.80	0.86	0.83
		500	1.00	0.80	0.87	2.25	0.99	0.82	0.88	2.20	0.99	0.83	0.88	1.52	0.99	0.94	0.97	0.42
		1000	1.00	0.91	0.93	3.10	1.00	0.92	0.93	2.85	1.00	0.92	0.93	1.71	1.00	0.99	0.99	0.90
random	100	0.95	0.41	0.56	1.50	0.91	0.53	0.65	1.52	0.91	0.54	0.66	1.31	0.91	0.60	0.72	0.80	
	200	0.99	0.58	0.71	1.61	0.95	0.68	0.78	1.67	0.95	0.69	0.78	1.37	0.95	0.80	0.86	0.83	
	500	1.00	0.80	0.87	2.25	0.99	0.82	0.88	2.20	0.99	0.83	0.88	1.52	0.99	0.94	0.97	0.42	
	1000	1.00	0.91	0.93	3.10	1.00	0.92	0.93	2.85	1.00	0.92	0.93	1.71	1.00	0.99	0.99	0.90	

Supplementary Table S7. Monte Carlo means of Precision (P), Recall (R),  $F_1$ -score, and runtime obtained by simulating 50 samples from three different types of graphs in Figure S2 ( $p = 100$ ), under zinb and NB node conditional distributions mean  $\mu = 5$ ;  $\theta = 0.5$ ;  $\pi = 0.7$  and levels of noise  $\mu_{noise} = 0.5$ . The levels of significance of tests  $\alpha = 2(1 - \Phi(n^{0.2}))$  for  $n = 500, 1000$ , and  $\alpha = 2(1 - \Phi(n^{0.225}))$  for  $n = 200$ .

models	type	$n$	PC-nb				PC-nbglm			
			P	R	$F_1$	time	P	R	$F_1$	time
zinb	scalefree	200	0.28	0.71	0.40	109.36	0.85	0.36	0.50	8.73
		500	0.44	0.92	0.59	54.89	0.96	0.75	0.84	14.90
		1000	0.55	0.97	0.70	118.11	1.00	0.88	0.93	27.77
	hub	200	0.15	0.42	0.22	195.42	0.47	0.07	0.12	8.33
		500	0.30	0.85	0.45	1115.44	0.87	0.31	0.45	26.17
		1000	0.43	0.99	0.60	1614.48	0.98	0.62	0.76	77.16
	random	200	0.40	0.63	0.49	85.50	0.82	0.20	0.32	8.04
		500	0.60	0.93	0.73	39.03	0.98	0.66	0.79	13.19
		1000	0.73	0.99	0.84	59.62	1.00	0.87	0.93	23.09
NB	scalefree	200	0.51	0.86	0.64	106.25	0.91	0.57	0.70	7.27
		500	0.56	0.97	0.71	477.96	0.97	0.84	0.90	13.37
		1000	0.69	1.00	0.81	447.78	1.00	0.92	0.95	25.92
	hub	200	0.40	0.70	0.51	403.94	0.67	0.13	0.21	6.81
		500	0.49	0.97	0.65	1605.72	0.93	0.49	0.64	26.28
		1000	0.63	1.00	0.77	2369.42	0.99	0.81	0.89	159.07
	random	200	0.54	0.80	0.64	40.06	0.93	0.45	0.60	6.73
		500	0.61	0.98	0.75	110.86	0.99	0.82	0.90	10.74
		1000	0.74	1.00	0.85	178.44	1.00	0.96	0.98	19.29

Gene set	
<b>Community 1:</b>	
1	GO_CELLS_RESPONSE_TO_DNA_DAMAGE_STIMULUS
2	GO_REGULATION_OF_CELL_CYCLE
3	GO_CARBOHYDRATE_HOMEOSTASIS
4	GO_RESPONSE_TO_CARBOHYDRATE
5	GO_PROCESS_UTILIZING_AUTOPHAGIC_MECHANISM
6	GO_REGULATION_OF_MITOTIC_CELL_CYCLE
7	GO_NEGATIVE_REGULATION_OF_CELL_CYCLE_PROCESS
8	GO_REGULATION_OF_AUTOPHAGY
9	GO_DNA_REPAIR
10	GO_REGULATION_OF_CELL_CYCLE_PHASE_TRANSITION
<b>Community 2:</b>	
1	GO_PROTEIN_DEMETHYLATION
2	GO_DEMETHYLATION
3	GO_REGULATION_OF_DNA_REPLICATION
4	GO_FOAM_CELL_DIFFERENTIATION
5	GO_HISTONE_H3_K4_DEMETHYLATION
6	GO_HISTONE_H3_K4_DEMETHYLATION_TRIMETHYL_H3_K4_SPECIFIC
7	GO_HISTONE_H3_K4_METHYLATION
8	GO_RIBONUCLEOPROTEIN_COMPLEX_SUBUNIT_ORGANIZATION
9	GO_REGULATION_OF_CHOLESTEROL_BIOSYNTHETIC_PROCESS
10	GO_STEROL_BIOSYNTHETIC_PROCESS
<b>Community 3:</b>	
1	GO_SCHWANN_CELL_DIFFERENTIATION
2	GO_REGULATION_OF_CELL_POPULATION_PROLIFERATION
3	GO_EPIDERMIS_DEVELOPMENT
4	GO_POSITIVE_REGULATION_OF_CELL_DEATH
5	GO_PERIPHERAL_NERVOUS_SYSTEM_DEVELOPMENT
6	GO_RAS_PROTEIN_SIGNAL_TRANSDUCTION
7	GO_EPITHELIUM_DEVELOPMENT
8	GO_NEGATIVE_REGULATION_OF_BMP_SIGNALING_PATHWAY
9	GO_REGULATION_OF_CELL_CYCLE
10	GO_APOPTOTIC_PROCESS
<b>Community 4:</b>	
1	GO_DNA_REPLICATION_INITIATION
2	GO_DNA_DEPENDENT_DNA_REPLICATION
3	GO_CELL_CYCLE_G1_S_PHASE_TRANSITION
4	GO_DNA_UNWINDING_INVOLVED_IN_DNA_REPLICATION
5	GO_DNA_GEOMETRIC_CHANGE
6	GO_CELL_CYCLE_PHASE_TRANSITION
7	GO_DNA_REPLICATION
8	GO_MITOTIC_CELL_CYCLE
9	GO_DNA_METABOLIC_PROCESS
10	GO_DNA_CONFORMATION_CHANGE

Supplementary Table S8. Top 10 enriched gene sets identified for each of the transcription factor communities in the HBC\* cell type.

Gene set	
<b>Community 1:</b>	
1	GO_REGULATION_OF_SIGNAL_TRANSDUCTION_BY_P53_CLASS_MEDIATOR
2	GO_DNA_REPLICATION_INITIATION
3	GO_HISTONE_PHOSPHORYLATION
4	GO_SIGNAL_TRANSDUCTION_BY_P53_CLASS_MEDIATOR
5	GO_DNA_REPLICATION
6	GO_SNRNA_TRANSCRIPTION
7	GO_NCRNA_TRANSCRIPTION
8	GO_TRANSCRIPTION_ELONGATION_FROM_RNA_POLYMERASE_II_PROMOTER
9	GO_POSITIVE_REGULATION_OF_CHROMOSOME_ORGANIZATION
10	GO_DNA_TEMPLATED_TRANSCRIPTION_ELONGATION
<b>Community 2:</b>	
1	GO_REGULATION_OF_CELL_POPULATION_PROLIFERATION
2	GO_REGULATION_OF_NOTCH_SIGNALING_PATHWAY
3	GO_RESPONSE_TO_NITROGEN_COMPOUND
4	GO_NEGATIVE_REGULATION_OF_SIGNALING
5	GO_CELLULAR_RESPONSE_TO_EXTERNAL_STIMULUS
6	GO_RESPONSE_TO_PEPTIDE
7	GO_RESPONSE_TO_STARVATION
8	GO_CELLULAR_RESPONSE_TO_STARVATION
9	GO_CARDIOVASCULAR_SYSTEM_DEVELOPMENT
10	GO_NOTCH_SIGNALING_PATHWAY
<b>Community 3:</b>	
1	GO_RNA_SPLICING_VIA_TRANSESTERIFICATION_REACTIONS
2	GO_REGULATION_OF_GENE_SILENCING
3	GO_RNA_SPLICING
4	GO_CELLULAR_PROTEIN_CONTAINING_COMPLEX_ASSEMBLY
5	GO_DNA_REPAIR
6	GO_MRNA_METABOLIC_PROCESS
7	GO_TRANSCRIPTION_PREINITIATION_COMPLEX_ASSEMBLY
8	GO_REGULATION_OF_GENE_EXPRESSION_EPIGENETIC
9	GO_REGULATION_OF_STEM_CELL_DIFFERENTIATION
10	GO_REGULATION_OF_DNA_BINDING
<b>Community 4:</b>	
1	GO_REGULATION_OF_NIK_NF_KAPPAB_SIGNALING
2	GO_ORGANELLE_LOCALIZATION
3	GO_NIK_NF_KAPPAB_SIGNALING
4	GO_ESTABLISHMENT_OF_ORGANELLE_LOCALIZATION
5	GO_MICROTUBULE_CYTOSKELETON_ORGANIZATION_INVOLVED_IN_MITOSIS
6	GO_POSITIVE_REGULATION_OF_NIK_NF_KAPPAB_SIGNALING
7	GO_SPINDLE_ASSEMBLY
8	GO_HISTONE_H3_ACETYLATION
9	GO_HISTONE_H4_ACETYLATION
10	GO_CELLULAR_RESPONSE_TO_CALCIUM_ION

Supplementary Table S9. Top 10 enriched gene sets identified for each of the transcription factor communities in the GBC cell type.



Gene set	
<b>Community 1:</b>	
1	GO_NEUROGENESIS
2	GO_TELENCEPHALON_DEVELOPMENT
3	GO_NEURON_DIFFERENTIATION
4	GO_EMBRYO_DEVELOPMENT
5	GO_REGULATION_OF_NERVOUS_SYSTEM_DEVELOPMENT
6	GO_REGULATION_OF_CELL_POPULATION_PROLIFERATION
7	GO_POSITIVE_REGULATION_OF_CELL_POPULATION_PROLIFERATION
8	GO_NEGATIVE_REGULATION_OF_NEURON_DIFFERENTIATION
9	GO_NEGATIVE_REGULATION_OF_GENE_EXPRESSION_EPIGENETIC
10	GO_FOREBRAIN_DEVELOPMENT
<b>Community 2:</b>	
1	GO_CELL_GROWTH
2	GO_DEVELOPMENTAL_CELL_GROWTH
3	GO_AXON_EXTENSION
4	GO_DEVELOPMENTAL_GROWTH_INVOLVED_IN_MORPHOGENESIS
5	GO_MAINTENANCE_OF_PROTEIN_LOCATION
6	GO_POSITIVE_REGULATION_OF_ESTABLISHMENT_OF_PROTEIN_LOCALIZATION
7	GO_NEURON_PROJECTION_EXTENSION
8	GO_REGULATION_OF_TRANSPORT
9	GO_REGULATION_OF_ESTABLISHMENT_OF_PROTEIN_LOCALIZATION
10	GO_RAB_PROTEIN_SIGNAL_TRANSDUCTION
<b>Community 3:</b>	
1	GO_RESPONSE_TO_TUMOR_NECROSIS_FACTOR
2	GO_REGULATION_OF_MRNA_CATABOLIC_PROCESS
3	GO_REGULATION_OF_STRESS_ACTIVATED_PROTEIN_KINASE_SIGNALING_CASCADE
4	GO_RESPONSE_TO_CYTOKINE
5	GO_RESPONSE_TO_WOUNDING
6	GO_REGULATION_OF_HISTONE_H3_K9_TRIMETHYLATION
7	GO_RESPONSE_TO_TYPE_I_INTERFERON
8	GO_WOUND_HEALING
9	GO_INTERFERON_GAMMA_MEDIATED_SIGNALING_PATHWAY
10	GO_TUMOR_NECROSIS_FACTOR_MEDIATED_SIGNALING_PATHWAY
<b>Community 4:</b>	
1	GO_REGULATION_OF_STEM_CELL_POPULATION_MAINTENANCE
2	GO_REGULATION_OF_DNA_TEMPLATED_TRANSCRIPTION_ELONGATION
3	GO_REGULATION_OF_PROTEIN_COMPLEX_ASSEMBLY
4	GO_REGULATION_OF_CELLULAR_AMIDE_METABOLIC_PROCESS
5	GO_PEPTIDE_BIOSYNTHETIC_PROCESS
6	GO_AMIDE_BIOSYNTHETIC_PROCESS
7	GO_DNA_TEMPLATED_TRANSCRIPTION_ELONGATION
8	GO_POSITIVE_REGULATION_OF_DNA_BINDING_TRANSCRIPTION_FACTOR_ACTIVITY
9	GO_CELLULAR_AMIDE_METABOLIC_PROCESS
10	GO_MAINTENANCE_OF_CELL_NUMBER

Supplementary Table S10. Top 10 enriched gene sets identified for each of the transcription factor communities in the iOSN cell type.

Gene set	
<b>Community 1:</b>	
1	GO_COVALENT_CHROMATIN_MODIFICATION
2	GO_CHROMATIN_ORGANIZATION
3	GO_PROTEIN_ACYLATION
4	GO_CHROMOSOME_ORGANIZATION
5	GO_RNA_SPLICING_VIA_TRANSESTERIFICATION_REACTIONS
6	GO_RRNA_TRANSCRIPTION
7	GO_POSITIVE_REGULATION_OF_DEFENSE_RESPONSE
8	GO_PROTEIN_ACETYLATION
9	GO_PEPTIDYL_LYSINE_ACETYLATION
10	GO_REGULATION_OF_RNA_SPLICING
<b>Community 2:</b>	
1	GO_ATP_DEPENDENT_CHROMATIN_REMODELING
2	GO_DNA_TEMPLATED_TRANSCRIPTION_ELONGATION
3	GO_PROTEIN_DNA_COMPLEX_SUBUNIT_ORGANIZATION
4	GO_FERTILIZATION
5	GO_RESPONSE_TO_EXTRACELLULAR_STIMULUS
6	GO_RESPONSE_TO_OSMOTIC_STRESS
7	GO_CHROMATIN_ORGANIZATION
8	GO_INSULIN_RECEPTOR_SIGNALING_PATHWAY
9	GO_ORGANOPHOSPHATE_BIOSYNTHETIC_PROCESS
10	GO_CELLULAR_PROCESS_INVOLVED_IN_REPRODUCTION_IN_MULTICELLULAR_ORGANISM
<b>Community 3:</b>	
1	GO_TRANSFORMING_GROWTH_FACTOR_BETA_RECEPTOR_SIGNALING_PATHWAY
2	GO_CELLULAR_RESPONSE_TO_INORGANIC_SUBSTANCE
3	GO_RESPONSE_TO_TRANSFORMING_GROWTH_FACTOR_BETA
4	GO_REGULATION_OF_DNA_BINDING
5	GO_NEURON_DEATH
6	GO_REGULATION_OF_DNA_TEMPLATED_TRANSCRIPTION_IN_RESPONSE_TO_STRESS
7	GO_TRANSMEMBRANE_RECEPTOR_PROTEIN_SERINE_THREONINE_KINASE_SIGNALING_PATHWAY
8	GO_POSITIVE_REGULATION_OF_NEURON_DEATH
9	GO_CELLULAR_RESPONSE_TO_CALCIIUM_ION
10	GO_RESPONSE_TO_METAL_ION
<b>Community 4:</b>	
1	GO_VIRAL_LIFE_CYCLE
2	GO_INTERSPECIES_INTERACTION_BETWEEN_ORGANISMS
3	GO_PROTEIN_MONOUBIQUITINATION
4	GO_REGULATION_OF_VIRAL_LIFE_CYCLE
5	GO_PROTEIN_MODIFICATION_BY_SMALL_PROTEIN_CONJUGATION
6	GO_REGULATION_OF_NUCLEAR_TRANSCRIBED_MRNA_CATABOLIC_PROCESS_DEADENYLATION_DEPENDENT_DE
7	GO_REGULATION_OF_SYMBIOSIS_ENCOMPASSING_MUTUALISM_THROUGH_PARASITISM
8	GO_PROTEIN_SUMOYLATION
9	GO_POSITIVE_REGULATION_OF_VIRAL_PROCESS
10	GO_CELLULAR_MACROMOLECULE_CATABOLIC_PROCESS
<b>Community 5:</b>	
1	GO_CELL_PROJECTION_ASSEMBLY
2	GO_REGULATION_OF_CIRCADIAN_RHYTHM
3	GO_NEGATIVE_REGULATION_OF_SMOOTHENED_SIGNALING_PATHWAY
4	GO_ENDOSOMAL_TRANSPORT
5	GO_POSITIVE_REGULATION_OF_CELL_CYCLE_G2_M_PHASE_TRANSITION
6	GO_SPINAL_CORD_PATTERNING
7	GO_PROTEIN_DEPHOSPHORYLATION
8	GO_PROTEIN_LOCALIZATION_TO_MEMBRANE
9	GO_CELL_CYCLE_G2_M_PHASE_TRANSITION
10	GO_MITOTIC_SISTER_CHROMATID_SEGREGATION

Supplementary Table S11. Top 10 enriched gene sets identified for each of the transcription factor communities in the mOSN cell type.

## REFERENCES

- ALLEN, G. AND LIU, Z. (2013). A local Poisson graphical model for inferring networks from sequencing data. *IEEE Transactions on Nanobioscience* **12**(3), 189–198.
- BROYDEN, C. G. (1970). The convergence of a class of double-rank minimization algorithms 1. general considerations. *IMA Journal of Applied Mathematics* **6**(1), 76–90.
- FLETCHER, R. (1970). A new approach to variable metric algorithms. *The computer journal* **13**(3), 317–322.
- FLETCHER, R. B., DAS, D., GADYE, L., STREET, K. N., BAUDHUIN, A., WAGNER, A., COLE, M. B., FLORES, Q., CHOI, Y. G., YOSEF, N. *and others.* (2017). Deconstructing olfactory stem cell trajectories at single-cell resolution. *Cell Stem Cell* **20**(6), 817–830.
- GOLDFARB, D. (1970). A family of variable metric updates derived by variational means, v. 24. *Mathematics of Computation* **24**(109), 23–26.
- LIBERZON, A., BIRGER, C., THORVALDSDÓTTIR, H., GHANDI, M., MESIROV, J. P. AND TAMAYO, P. (2015, dec). The Molecular Signatures Database Hallmark Gene Set Collection. *Cell Systems* **1**(6), 417–425.
- NGUYEN, T. K. H. AND CHIOGNA, M. (2018). Structure learning of undirected graphical models for count data. *ArXiv*, 1810.10854.
- RISSE, D., PERRAUDEAU, F., GRIBKOVA, S., DUDOIT, S. AND VERT, J. P. (2018). A general and flexible method for signal extraction from single-cell rna-seq data. *Nature Communications* **9**(1), 1–17.
- SHANNO, D. F. (1970). Conditioning of quasi-newton methods for function minimization. *Mathematics of computation* **24**(111), 647–656.
- SUBRAMANIAN, A., TAMAYO, P., MOOTHA, V. K., MUKHERJEE, S., EBERT, B. L., GILLETTE, M. A., PAULOVICH, A., POMEROY, S. L., GOLUB, T. R., LANDER, E. S. *and others.* (2005). Gene set enrichment analysis: A knowledge-based approach for interpreting genome-wide expression profiles. *Proceedings of the National Academy of Sciences* **102**(43), 15545–15550.
- TRAAG, V. A., WALTMAN, L. AND VAN ECK, N. J. (2019). From Louvain to Leiden: guaranteeing well-connected communities. *Scientific Reports* **9**(1), 5233.